



Institut für Numerische Simulation
Rheinische Friedrich-Wilhelms-Universität Bonn

Wegelerstraße 6 • 53115 Bonn • Germany
phone +49 228 73-3427 • fax +49 228 73-7527
www.ins.uni-bonn.de

Paul Hennig
Markus Kästner
Philipp Morgenstern
Daniel Peterseim

Adaptive Mesh Refinement Strategies in Isogeometric Analysis - A Computational Comparison

INS Preprint No. 1611

May 2016

Adaptive Mesh Refinement Strategies in Isogeometric Analysis - A Computational Comparison*

Paul Hennig^a, Markus Kästner^a,
Philipp Morgenstern^b, Daniel Peterseim^b

May 3, 2016

We explain four variants of an adaptive finite element method with cubic splines and compare their performance in simple elliptic model problems. The methods in comparison are Truncated Hierarchical B-splines with two different refinement strategies, T-splines with the refinement strategy introduced by Scott et al. in 2012, and T-splines with an alternative refinement strategy introduced by some of the authors. In four examples, including singular and non-singular problems of linear elasticity and the Poisson problem, the H1-errors of the discrete solutions, the number of degrees of freedom as well as sparsity patterns and condition numbers of the discretized problem are compared.

1 Introduction

Adaptive Isogeometric Methods (AIGM) have gained widespread interest and are a very active field of research, investigating a wide range of refinement strategies. The “usual” mesh refinement, entitled h -refinement, currently competes with p -refinement (augmenting the polynomial degree), k -refinement (a particular combination of h - and p -refinement), r -refinement (redesigning the mesh) and their combinations. However, if B-splines or NURBS are considered as a basis, their tensor product nature will prohibit a truly local h -refinement within a single patch, and various approaches have been developed to overcome this restrictive tensor product structure.

The concept of T-splines as an h -refinement technique caught much attention [1, 2], but also incorporated algorithmic difficulties [3], in particular linear dependencies between the T-spline functions that should serve as a spline basis, and an unclear nesting behaviour of the generated spline spaces. Most of these problems could be solved in the last years [4, 5, 6, 7, 8, 9].

Hierarchical (H)B-splines, a further promising h -refinement technique, have been introduced already in 1988 [10] and developed to meet the requirements of isogeometric analysis [11, 12, 13]. They have been enhanced to truncated hierarchical (TH)B-splines [14] by reducing the interaction between basis functions of different refinement levels. As a result, THB-splines improve the conditioning and reduce the bandwidth as well as the total number of non-zero entries in the system matrices [15, 16]. The mentioned interaction can be further regulated by the introduction of m -admissible meshes, where interacting basis functions in an element belong to at most m different levels [17].

Further h -refinement techniques are locally refined (LR-)B-splines [18, 19], hierarchical T-splines [20], modified T-splines [21], PHT-splines [22, 23] amongst many others.

In this contribution, four different realizations of an Adaptive Isogeometric Method with h -refinement are compared:

*The authors gratefully acknowledge support by the Deutsche Forschungsgemeinschaft in the Priority Program 1748 “Reliable simulation techniques in solid mechanics: Development of non-standard discretization methods, mechanical and mathematical analysis” under the project “Adaptive isogeometric modeling of propagating strong discontinuities in heterogeneous materials” (KA3309/3-1 and PE2143/2-1).

^aTechnische Universität Dresden, Institute for Solid Mechanics,
George-Bähr-Straße 3c, 01062 Dresden, Germany
email addresses: paul.hennig@tu-dresden.de, markus.kaestner@tu-dresden.de

^bRheinische Friedrich-Wilhelms-Universität Bonn, Institute for Numerical Simulation,
Wegelerstr. 6, 53115 Bonn, Germany
email addresses: morgenstern@ins.uni-bonn.de, peterseim@ins.uni-bonn.de

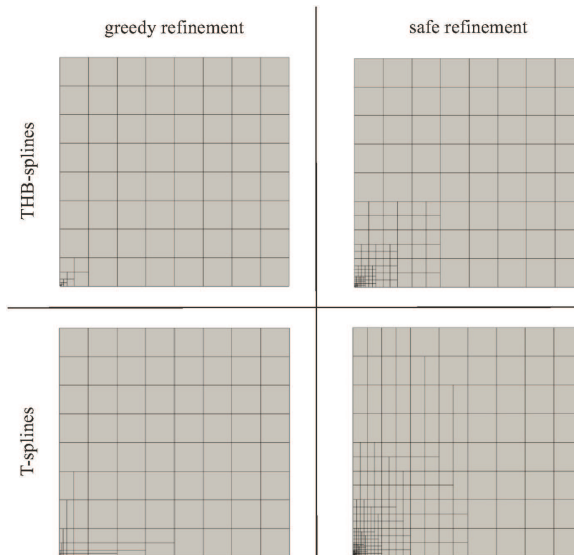


Figure 1: Refinement strategies: An initial square mesh with 64 elements is locally refined in the lower left corner using THB- and T-splines with a greedy and a safe refinement. The illustrated meshes are the Bézier meshes (see Definition 2.15).

1. A refinement based on T-splines [6], where the refinement process is divided into two steps. At first, marked elements are refined, and secondly, an additional refinement is processed to recover the linear independence of the T-spline functions, called *analysis-suitability*.
2. A refinement based on T-splines [9, 8], where also the vicinity of the marked elements is considered. By defining a class of admissible T-meshes, the proposed refinement preserves the analysis-suitability of the T-splines directly.
3. A refinement based on THB-splines, where the mesh allows only a one-level difference between neighbouring mesh elements.
4. A refinement based on THB-splines, where only 2-admissible meshes are allowed.

We refer to these methods as *greedy refinement* (method 1 and 3) and *safe refinement* (method 2 and 4).

Some of these methods allow for a mathematical proof of linear complexity [24, 8]. Together with results on the convergence of the Adaptive Algorithm [17], this allows for a proof of optimal convergence rates [25]. This paper will compare the refinement of T-splines and THB-splines with a focus on the influence of the different mesh classes on the numerical solution and properties. In four examples, including singular and non-singular problems of linear elasticity and the Poisson problem, the H1-errors of the discrete solutions, the number of degrees of freedom as well as sparsity patterns and condition numbers of the discretized problem are compared.

To enable a unified implementation of the different refinement techniques, Bézier extraction is used. Bézier extraction provides a canonical form to use isogeometric analysis with different spline bases, has a strict element viewpoint, allows for an implementation into existing finite element codes and has been already developed for T-splines [26] and THB-splines [27].

The paper is organized as follows. Section 2 introduces the refinement strategies to be compared. Section 3 describes the problems that will be solved numerically using each of the presented methods. Section 4 investigates the adaptive algorithm and summarizes background theory on optimal convergence rates. The computational comparison is performed in Section 5, and conclusions are given in Section 6.

2 Mesh Refinement Strategies

In this section, we define several h -refinement strategies for bivariate B-splines. They will be described in the style

$$\text{REFINE}(Q, \mathcal{M}) = (\tilde{Q}, \tilde{\mathcal{B}}),$$

with Q being a rectangular mesh in the index domain and $\mathcal{M} \subseteq Q$ a set of elements (rectangles) to be refined. \tilde{Q} and $\tilde{\mathcal{B}}$ are the new refined mesh and the set of B-spline basis functions associated to that new mesh, respectively.

2.1 Uniform refinement

We assume the initial mesh \mathcal{Q}_0 to be a tensor product mesh, and its elements are closed squares with side length 1 (see Figure 2),

$$\mathcal{Q}_0 := \left\{ [m-1, m] \times [n-1, n] \mid m \in \{1, \dots, M\}, n \in \{1, \dots, N\} \right\}.$$

The corresponding spline basis \mathcal{B}_0 is spanned by the corresponding tensor-product B-splines. For each level $k \in \mathbb{N}_0$, we define the tensor-product mesh

$$\mathcal{Q}_k := \left\{ [x-2^{-k}, x] \times [y-2^{-k}, y] \mid 2^k x \in \{1, \dots, 2^k M\}, 2^k y \in \{1, \dots, 2^k N\} \right\}$$

and the corresponding spline space \mathcal{B}_k of tensor-product bivariate B-spline basis functions.

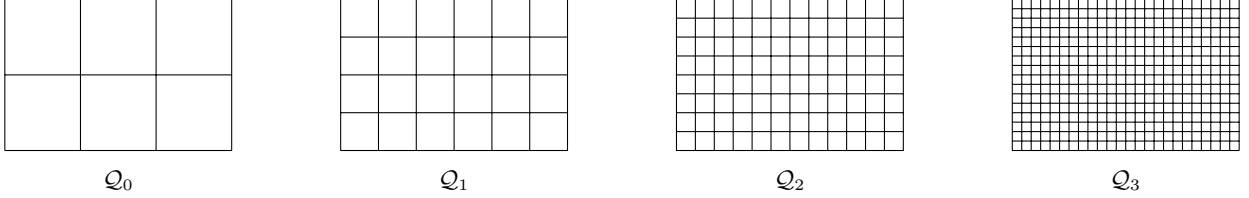


Figure 2: Example for the uniform meshes $\mathcal{Q}_0, \dots, \mathcal{Q}_3$ for $M = 3$ and $N = 2$.

Definition 2.1. We define the uniform refinement routine by

$$\text{REFINE_UNIFORM}(\mathcal{Q}_k, \mathcal{M}) := (\mathcal{Q}_{k+1}, \mathcal{B}_{k+1}) \quad \text{for any } k \in \mathbb{N}_0 \text{ and } \mathcal{M} \subseteq \mathcal{Q}.$$

Note that the set of marked elements \mathcal{M} enters only for formal reasons and has no effect on the refinement. We denote the class of uniform meshes by $\mathbb{M}_{\text{UNIFORM}} := \{\mathcal{Q}_n \mid n \in \mathbb{N}_0\}$.

Definition 2.2 (level). Given $k \in \mathbb{N}$ and $q \in \mathcal{Q}_k$, we denote the *level* of q by $\ell(q) := k$.

2.2 Truncated Hierarchical B-splines

For the use of Truncated Hierarchical B-splines (THB-splines), the underlying rectangular mesh \mathcal{Q} may consist of finitely many elements from meshes in $\mathbb{M}_{\text{UNIFORM}}$, such that any two elements of \mathcal{Q} have disjoint interior, and the union of all elements of \mathcal{Q} is the same domain $[0, M] \times [0, N]$ that is covered by uniform meshes. In particular, \mathcal{Q} is meant to contain elements of different levels:

$$\mathbb{M}_{\text{THB}} := \left\{ \mathcal{Q} \subset \bigcup_{\mathcal{Q}' \in \mathbb{M}_{\text{UNIFORM}}} \mathcal{Q}' \mid \#\mathcal{Q} < \infty, \bigcup \mathcal{Q} = [0, M] \times [0, N], \forall q, q' \in \mathcal{Q} : \text{int}(q) \cap \text{int}(q') = \emptyset \right\}.$$

Definition 2.3 (level- k domain). Given some mesh $\mathcal{Q} \in \mathbb{M}_{\text{THB}}$, and $k \in \mathbb{N}_0$, we denote by $\Omega_{\mathcal{Q}, k}$ the domain that is covered by “level- k or finer” elements, $\Omega_{\mathcal{Q}, k} := \bigcup \{q \in \mathcal{Q} \mid \ell(q) \geq k\}$. See Figure 3 for an example.

The classical (non-truncated) Hierarchical B-spline basis reads

$$\mathcal{B}_{\text{HB}}^{\mathcal{Q}} := \bigcup_{k \in \mathbb{N}_0} \{B \in \mathcal{B}_k \mid \text{supp } B \subseteq \Omega_{\mathcal{Q}, k} \text{ and } \text{supp } B \not\subseteq \Omega_{\mathcal{Q}, k+1}\}.$$

THB-splines involve an alternative choice of basis functions that span the same space as the basis $\mathcal{B}_{\text{HB}}^{\mathcal{Q}}$ above. These basis functions have reduced overlap compared to $\mathcal{B}_{\text{HB}}^{\mathcal{Q}}$ and hence provide sparser Galerkin and Collocation matrices when used for solving a discretized PDE.

Definition 2.4 (Truncation of the classical basis, [14]). Let $B = \sum_{\bar{B} \in \mathcal{B}_j} c_{\bar{B}, B} \bar{B} \in \text{span } \mathcal{B}_j$, then

$$\text{trunc}_{\mathcal{Q}}^j(B) := \sum_{\bar{B} \in \mathcal{B}_j \setminus \mathcal{B}_{\text{HB}}^{\mathcal{Q}}} c_{\bar{B}, B} \bar{B}.$$

In addition, for any $B \in \mathcal{B}_k$, $k \in \mathbb{N}_0$ we define the successive truncation w.r.t. all higher levels

$$\text{Trunc}_{\mathcal{Q}}(B) := \text{trunc}_{\mathcal{Q}}^K(\dots \text{trunc}_{\mathcal{Q}}^{k+2}(\text{trunc}_{\mathcal{Q}}^{k+1}(B)) \dots)$$

with $K = \max\{k \in \mathbb{N}_0 \mid \mathcal{B}_k \cap \mathcal{B}_{\text{HB}}^{\mathcal{Q}} \neq \emptyset\}$.

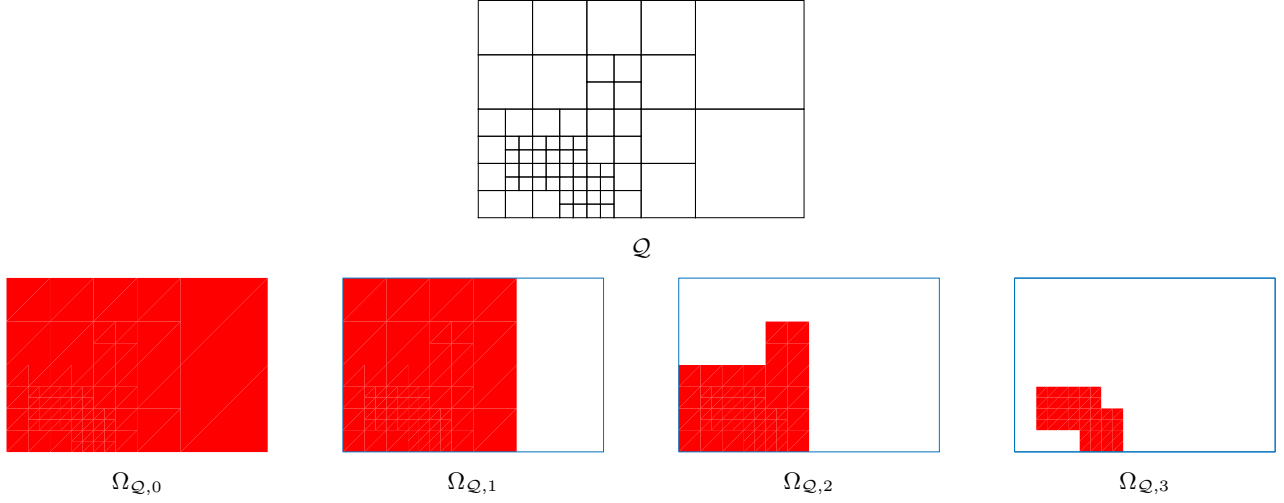


Figure 3: Example for level- k domains, for $k = 0, \dots, 3$. The domains $\Omega_{\mathcal{Q},0}, \dots, \Omega_{\mathcal{Q},3}$ are shaded in red.

Definition 2.5 (Subdivision). For $k \in \mathbb{N}_0$ and $q \in \mathcal{Q}_k$, we define

$$\text{SUBDIVIDE}(q) := \{q' \in \mathcal{Q}_{k+1} \mid q' \subset q\}$$

and for $\mathcal{M} \subset \mathcal{Q} \in \mathbb{M}_{\text{THB}}$, we denote $\text{SUBDIVIDE}(\mathcal{M}) := \bigcup_{q \in \mathcal{M}} \text{SUBDIVIDE}(q)$.

Definition 2.6. The refinement procedure for THB-splines reads $\text{REFINE_THB}(\mathcal{Q}, \mathcal{M}) := (\tilde{\mathcal{Q}}, \mathcal{B}_{\text{THB}}^{\tilde{\mathcal{Q}}})$, with

$$\begin{aligned} \tilde{\mathcal{Q}} &:= \mathcal{Q} \setminus \mathcal{M} \cup \text{SUBDIVIDE}(\mathcal{M}) \\ \mathcal{B}_{\text{THB}}^{\tilde{\mathcal{Q}}} &:= \left\{ \text{Trunc}(B) \mid B \in \mathcal{B}_{\text{THB}}^{\mathcal{Q}} \right\}. \end{aligned}$$

2.2.1 Greedy refinement for THB-Splines

The greedy THB-spline refinement defined below allows only a one-level difference between neighbouring mesh elements to produce graded meshes. Examples are given in Figure 4 and Figure 5.

Definition 2.7 (Greedy refinement for THB-Splines). We define for each $q \in \mathcal{Q}$ the *coarse neighbourhood*

$$\mathcal{N}_{\text{THB}^+}(q) := \{q' \in \mathcal{Q} \mid \ell(q') > \ell(q), q \cap q' \neq \emptyset\}$$

with generalized notations $\mathcal{N}_{\text{THB}^+}(\mathcal{M}) := \bigcup_{q \in \mathcal{M}} \mathcal{N}_{\text{THB}^+}(q)$ and $\mathcal{N}_{\text{THB}^+}^k(\mathcal{M}) := \underbrace{\mathcal{N}_{\text{THB}^+}(\dots \mathcal{N}_{\text{THB}^+}(\mathcal{M}) \dots)}_{k \text{ times}}$. We further define the *closure*

$$\text{CLOSURE_THB}^+(\mathcal{M}, \mathcal{Q}) := \bigcup_{k=0}^{\max \ell(\mathcal{M})} \mathcal{N}_{\text{THB}^+}^k(\mathcal{M}),$$

and the extended refinement procedure

$$\text{REFINE_THB}^+(\mathcal{Q}, \mathcal{M}) := \text{REFINE_THB}(\mathcal{Q}, \text{CLOSURE_THB}^+(\mathcal{M}, \mathcal{Q})).$$

2.2.2 Safe refinement for THB-Splines

The safe refinement for THB-splines defined below is conceptionally similar to the refinement procedure described in [17] and [24]. It only differs in the construction of the neighbourhood $\mathcal{N}_{\text{THB}^{++}}$, where a different level is chosen for the B-splines whose supports are used in the construction. The resulting meshes are 2-admissible, meaning that interacting basis functions in an element belong to at most two different levels. Examples are given in Figure 6 and Figure 7.

Definition 2.8 (Safe refinement for THB-Splines). We define for each $q \in \mathcal{Q}$ the *same-level neighbourhood*

$$\mathcal{N}_{\text{SL}}(q) := \{q' \in \mathcal{Q}_{\ell(q)} \mid \exists B \in \mathcal{B}_{\ell(q)} : q \subset \text{supp } B \supset q'\},$$

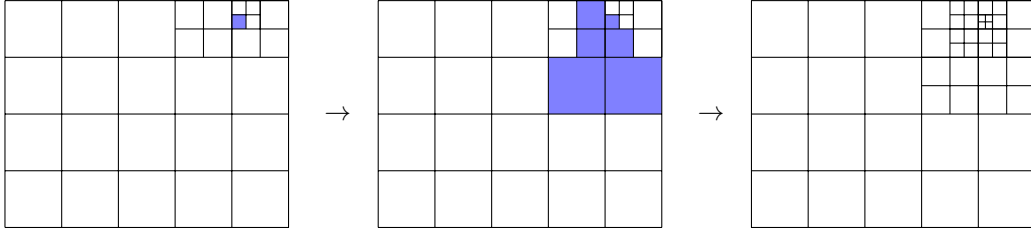


Figure 4: Example for the greedy THB-spline refinement. First, an element $q \in \mathcal{Q}$ is marked (highlighted in blue), hence $\mathcal{M} = \{q\}$. Second, $\text{CLOSURE_THB}^+(\mathcal{M}, \mathcal{Q})$ is computed (highlighted in blue). Third, all elements in $\text{CLOSURE_THB}^+(\mathcal{M}, \mathcal{Q})$ are subdivided.

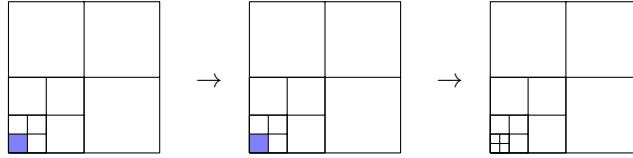


Figure 5: Another example for the greedy THB-spline refinement. First, an element $q \in \mathcal{Q}$ is marked (highlighted in blue), hence $\mathcal{M} = \{q\}$. Second, $\text{CLOSURE_THB}^+(\mathcal{M}, \mathcal{Q})$ is computed, which now coincides with the actually marked element. Third, all elements in $\text{CLOSURE_THB}^+(\mathcal{M}, \mathcal{Q})$ are subdivided, which is only q .

the *coarse neighbourhood*

$$\mathcal{N}_{\text{THB}^{++}}(q) := \{q' \in \mathcal{Q} \mid \ell(q') < \ell(q), \exists q'' \in \mathcal{N}_{\text{SL}}(q) : q'' \subset q'\},$$

the *closure*

$$\text{CLOSURE_THB}^{++}(\mathcal{M}, \mathcal{Q}) := \bigcup_{k=0}^{\max \ell(\mathcal{M})} \mathcal{N}_{\text{THB}^{++}}^k(\mathcal{M}),$$

and the extended refinement procedure

$$\text{REFINE_THB}^{++}(\mathcal{Q}, \mathcal{M}) := \text{REFINE_THB}(\mathcal{Q}, \text{CLOSURE_THB}^{++}(\mathcal{M}, \mathcal{Q})).$$

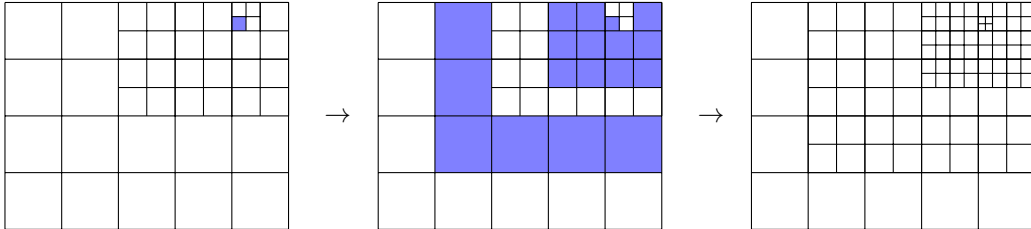


Figure 6: Example for the safe THB-spline refinement. First, an element $q \in \mathcal{Q}$ is marked (highlighted in blue), hence $\mathcal{M} = \{q\}$. Second, $\text{CLOSURE_THB}^+(\mathcal{M}, \mathcal{Q})$ is computed (highlighted in blue). Third, all elements in $\text{CLOSURE_THB}^+(\mathcal{M}, \mathcal{Q})$ are subdivided.

2.3 T-splines

While the refinement strategies for THB-splines presented above differ only in the choice of the neighbourhoods $\mathcal{N}_{\text{THB}^+}$ and $\mathcal{N}_{\text{THB}^{++}}$, the refinement strategies for T-splines below are conceptionally different. Throughout this paper, we denote the refinement procedure introduced in [6] as *greedy refinement for T-splines*. It relies on T-junctions and T-junction extensions, and the set of children from a single element's bisection may be any set of two rectangles with disjoint interior such that their union is the parent element. This is, any element can be bisected in *both* x - or y -direction, and the children may differ in size from each other. On the other hand, the refinement strategy from [8], denoted *safe refinement for T-splines*, follows the structure of the THB-spline refinement above, marking coarser elements in the neighbourhood of marked elements, and then refining all marked elements at the same time. For the safe refinement, each element can be bisected in *either* x - or y -direction, producing two rectangles with equal size, i.e., each element has a unique fixed set of children.

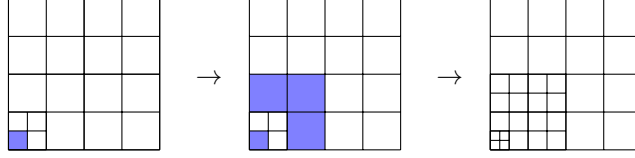


Figure 7: Another example for the safe THB-spline refinement. First, an element $Q \in \mathcal{Q}$ is marked (highlighted in blue), hence $\mathcal{M} = \{Q\}$. Second, $\text{CLOSURE_THB}^+(\mathcal{M}, \mathcal{Q})$ is computed. Third, all elements in $\text{CLOSURE_THB}^+(\mathcal{M}, \mathcal{Q})$ are subdivided.

For the sake of legibility, we only give a definition of odd-degree T-splines. However, both refinement procedures REFINE_TSPLINE^+ and $\text{REFINE_TSPLINE}^{++}$ are also suitable for even- or mixed-degree T-splines [6, 8, 28].

2.3.1 Greedy refinement for T-splines

Definition 2.9. For any rectangle $Q = [x, x + \tilde{x}] \times [y, y + \tilde{y}]$ and parameters $j \in \{1, 2\}$, $0 < q < 1$, we define the refinement

$$\text{BISECT}_{j,q}(Q) := \begin{cases} \{[x, x + q\tilde{x}] \times [y, y + \tilde{y}], [x + q\tilde{x}, x + \tilde{x}] \times [y, y + \tilde{y}]\} & \text{if } j = 1, \\ \{[x, x + \tilde{x}] \times [y, y + q\tilde{y}], [x, x + \tilde{x}] \times [y + q\tilde{y}, y + \tilde{y}]\} & \text{if } j = 2. \end{cases}$$



Figure 8: Example for $\text{BISECT}_{j,q}$.

Definition 2.10. We define the mesh class $\mathbb{M}_{\text{TSPLINE}}$ inductively through the $\text{BISECT}_{j,q}$ routine;

$$\begin{aligned} & \mathcal{Q}_0 \in \mathbb{M}_{\text{TSPLINE}}, \text{ and} \\ & \forall \mathcal{Q} \in \mathbb{M}_{\text{TSPLINE}} \quad \forall Q \in \mathcal{Q}, \quad j \in \{1, 2\}, \quad 0 < q < 1 : \quad (\mathcal{Q} \setminus \{Q\} \cup \text{BISECT}_{j,q}(Q)) \in \mathbb{M}_{\text{TSPLINE}}. \end{aligned}$$

Definition 2.11 (Skeleton). Given a mesh $\mathcal{Q} \in \mathbb{M}_{\text{TSPLINE}}$ and $Q = [x, x + \tilde{x}] \times [y, y + \tilde{y}] \in \mathcal{Q}$, we denote the union of all vertical (resp. horizontal) element sides by

$$\begin{aligned} \text{vSk}(Q) &:= [x, x + \tilde{x}] \times [y, y + \tilde{y}], \\ \text{hSk}(Q) &:= [x, x + \tilde{x}] \times \{y, y + \tilde{y}\}, \\ \text{vSk}(\mathcal{Q}) &:= \bigcup_{Q \in \mathcal{Q}} \text{vSk}(Q), \quad \text{hSk}(\mathcal{Q}) := \bigcup_{Q \in \mathcal{Q}} \text{hSk}(Q). \end{aligned}$$

We call vSk the *vertical skeleton* and hSk the *horizontal skeleton*.

Definition 2.12 (Vertices and T-junctions). For any mesh $\mathcal{Q} \in \mathbb{M}_{\text{TSPLINE}}$ and element $Q = [x, x + \tilde{x}] \times [y, y + \tilde{y}] \in \mathcal{Q}$, we define the set of *vertices*

$$\mathbf{V}(Q) := \{x, x + \tilde{x}\} \times \{y, y + \tilde{y}\}, \text{ and } \mathbf{V}(\mathcal{Q}) := \bigcup_{Q \in \mathcal{Q}} \mathbf{V}(Q).$$

We denote as *T-junction* each vertex that is in an element without being a vertex of it,

$$\mathbf{T}(Q) := \mathbf{V}(\mathcal{Q}) \cap Q \setminus \mathbf{V}(Q), \text{ and } \mathbf{T}(\mathcal{Q}) := \bigcup_{Q \in \mathcal{Q}} \mathbf{T}(Q).$$

Note that the above union is disjoint, i.e., for any T-junction $v \in \mathbf{T}(\mathcal{Q})$ there is a *unique* element $Q_v \in \mathcal{Q}$ such that $v \in \mathbf{T}(Q_v)$. We distinguish horizontal and vertical T-junctions. A T-junction is called *horizontal* if it is in a vertical side of the corresponding element, and *vertical* if it is in a horizontal side,

$$\begin{aligned} \mathbf{T}_h(Q) &:= \{v \in \mathbf{T}(Q) \mid v \in \text{vSk}(Q)\}, \\ \mathbf{T}_v(Q) &:= \{v \in \mathbf{T}(Q) \mid v \in \text{hSk}(Q)\}, \\ \mathbf{T}_h(\mathcal{Q}) &:= \bigcup_{Q \in \mathcal{Q}} \mathbf{T}_h(Q), \quad \mathbf{T}_v(\mathcal{Q}) := \bigcup_{Q \in \mathcal{Q}} \mathbf{T}_v(Q). \end{aligned}$$

Note that $\mathbf{T}_h(\mathcal{Q})$ and $\mathbf{T}_v(\mathcal{Q})$ are disjoint and $\mathbf{T}_h(\mathcal{Q}) \cup \mathbf{T}_v(\mathcal{Q}) = \mathbf{T}(\mathcal{Q})$.

Definition 2.13. For any $v = (v_1, v_2) \in [0, M] \times [0, N]$, we define

$$\begin{aligned} X(v) &:= \{z \in \mathbf{vSk} \mid z_2 = v_2\} \cup \{-\lceil \frac{p}{2} \rceil, \dots, -1, M+1, \dots, M + \lceil \frac{p}{2} \rceil\} \times \{y\}, \\ Y(v) &:= \{z \in \mathbf{hSk} \mid z_1 = v_1\} \cup \{x\} \times \{-\lceil \frac{q}{2} \rceil, \dots, -1, N+1, \dots, N + \lceil \frac{q}{2} \rceil\}. \end{aligned}$$

Remark. The above-defined sets $X(y)$ and $Y(x)$ are sets of points, in contrast to the literature, where they are defined as sets of indices and referred to as “global index sets” [8] or “global index vectors” [6].

Definition 2.14 (T-junction extensions). For any T-junction $v \in \mathbf{T}(\mathcal{Q})$, we define the T-junction extension as follows. Consider $X(v)$ to be ordered with respect to the first coordinate, then $\mathbf{x}_{\text{ext}}(v)$ is defined as the unique set of $p_1 + 1$ consecutive elements of $X(v)$ having the two elements of $X(v) \cap Q_v$ as the two middle entries. We denote by $\text{conv}(\mathbf{x}_{\text{ext}}(v))$ the convex hull of these points. Analogously, let $Y(v)$ be ordered with respect to the second coordinate, and $\mathbf{y}_{\text{ext}}(v)$ the unique set of $p_2 + 1$ elements of $Y(v)$ having the two elements of $Y(v) \cap Q_v$ as the two middle entries, and $\text{conv}(\mathbf{y}_{\text{ext}}(v))$ the convex hull of these points. The *T-junction extension* of v is defined as

$$\text{ext}_{\mathcal{Q}}(v) := \begin{cases} \text{conv}(\mathbf{x}_{\text{ext}}(v)) & \text{if } v \in \mathbf{T}_h(\mathcal{Q}), \\ \text{conv}(\mathbf{y}_{\text{ext}}(v)) & \text{if } v \in \mathbf{T}_v(\mathcal{Q}). \end{cases}$$

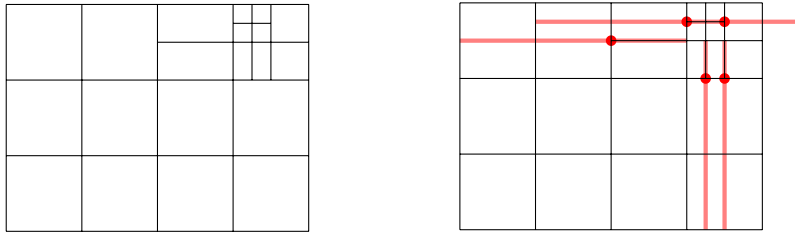


Figure 9: Example for T-junction extensions. The left figure show the considered mesh, and the right figure shows the same mesh with indicated T-junctions (red bullets) and the corresponding T-junction extensions (light red thick lines).

Definition 2.15 (Bézier mesh). Given a mesh $\mathcal{Q} \in \mathbb{M}_{\text{TSPLINE}}$, adding all T-junction extensions as actual edges to \mathcal{Q} yields the *Bézier mesh*, also called *extended T-mesh*. It represents the lowest-dimensional piecewise polynomial space that contains $\mathcal{B}_{\text{TSPLINE}}^{\mathcal{Q}}$ and is used for mesh comparisons in this paper, see e.g. Figure 1.

Definition 2.16 (T-spline functions). To each active node $v = (v_1, v_2) \in \mathbf{V}(\mathcal{Q})$, we associate a local index vector $\mathbf{x}(v) \in \mathbb{R}^{p+2}$, which is obtained by taking the unique $p+2$ consecutive elements in $X(v_2)$ having v_1 as their $\frac{p+3}{2}$ -th (this is, the middle) entry. We analogously define $\mathbf{y}(v) \in \mathbb{R}^{q+2}$.

We associate to each active node $v \in \mathbf{V}(\mathcal{Q})$ a bivariate B-spline function defined as the product of the one-dimensional B-spline functions on the corresponding local index vectors,

$$B_v(x, y, z) := N_{\mathbf{x}(v)}(x) \cdot N_{\mathbf{y}(v)}(y).$$

Given a mesh $\mathcal{Q} \in \mathbb{M}_{\text{TSPLINE}}$, the associated set of T-spline functions is defined by

$$\mathcal{B}_{\text{TSPLINE}}^{\mathcal{Q}} := \{B_v \mid v \in \mathbf{V}(\mathcal{Q})\}.$$

It is known from the literature that these functions are linearly independent if and only if there is no intersection between a horizontal and a vertical T-junction extension [4, 5]. Moreover, given a mesh $\mathcal{Q} \in \mathbb{M}_{\text{TSPLINE}}$ and a refinement $\tilde{\mathcal{Q}}$ thereof, the corresponding spline spaces are only nested if each T-junction extension is either eliminated or unchanged [7].

Definition 2.17. For any T-junction $v \in \mathbf{T}(\mathcal{Q})$, we denote by

$$\text{REFINE_TJUNC}(\mathcal{Q}, v) := \mathcal{Q} \setminus \{Q_v\} \cup \text{BISECT}_{j,q}(Q_v)$$

the single-element refinement such that $v \notin \mathbf{T}(\text{REFINE_TJUNC}(\mathcal{Q}, v))$, i.e., such that v is not a T-junction anymore.

Remark. This refinement exists and is unique, and it is constructed as follows. The definition of T-junctions states that there is exactly one element $Q_v \in \mathcal{Q}$ such that $v \in \mathbf{T}(Q_v)$. The location of v on the boundary of Q_v uniquely defines bisection parameters j and q such that v is a vertex of each children $Q' \in \text{BISECT}_{j,q}(Q_v)$.

Definition 2.18 (Extension crossing, extension incompatibility). For any mesh $\mathcal{Q} \in \mathbb{M}_{\text{TSPLINE}}$, we denote the set of *extension-crossing T-junction pairs* by

$$E(\mathcal{Q}) := \{(v, w) \in \mathbb{T}_h(\mathcal{Q}) \times \mathbb{T}_v(\mathcal{Q}) \mid \text{ext}_{\mathcal{Q}}(v) \cap \text{ext}_{\mathcal{Q}}(w) \neq \emptyset\}.$$

For any mesh $\mathcal{Q} \in \mathbb{M}_{\text{TSPLINE}}$ and refinement $\tilde{\mathcal{Q}} \in \mathbb{M}_{\text{TSPLINE}}$, we define the set of *extension-incompatible T-junctions* by

$$C(\mathcal{Q}, \tilde{\mathcal{Q}}) := \{v \in \mathbb{T}(\mathcal{Q}) \cap \mathbb{T}(\tilde{\mathcal{Q}}) \mid \text{ext}_{\tilde{\mathcal{Q}}}(v) \not\subseteq \text{ext}_{\mathcal{Q}}(v)\}.$$

Algorithm 2.19 (Greedy refinement for T-splines, [6]).

Require: mesh $\mathcal{Q} \in \mathbb{M}_{\text{TSPLINE}}$, marked elements $\mathcal{M} \subset \mathcal{Q}$

$\tilde{\mathcal{Q}} := \text{REFINE_THB}(\mathcal{Q}, \mathcal{M})$

repeat

$$v_{\text{refine}} := \underset{v \in \mathbb{T}(\tilde{\mathcal{Q}})}{\text{argmin}} \left(\#E(\text{REFINE_TJUNC}(\tilde{\mathcal{Q}}, v)) + \#C(\mathcal{Q}, \text{REFINE_TJUNC}(\tilde{\mathcal{Q}}, v)) \right)$$

$$\tilde{\mathcal{Q}} := \text{REFINE_TJUNC}(\tilde{\mathcal{Q}}, v_{\text{refine}})$$

until $E(\tilde{\mathcal{Q}}) = \emptyset$ and $C(\mathcal{Q}, \tilde{\mathcal{Q}}) = \emptyset$

return $\text{REFINE_TSPLINE}^+(\mathcal{Q}, \mathcal{M}) := (\tilde{\mathcal{Q}}, \mathcal{B}_{\text{TSPLINE}}^{\tilde{\mathcal{Q}}})$

Remark. The above algorithm does always finish, in the worst case yielding a tensor-product mesh.

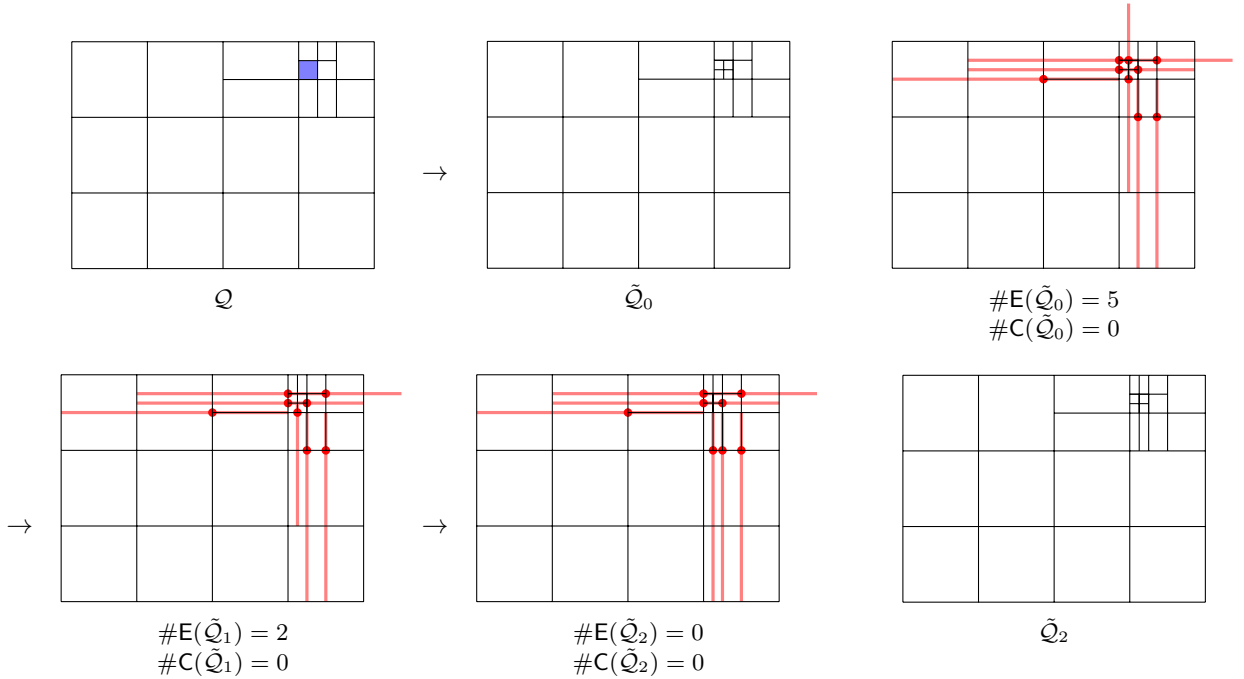


Figure 10: Example for the greedy T-spline refinement. In the first step, the marked element is subdivided as for the THB-spline refinement. Second, the intersections of horizontal and vertical T-junction extensions are counted. Third, REFINE_TJUNC is applied to a T-junction for which the number of extension crossings in the resulting mesh (elements of $E(\tilde{\mathcal{Q}})$) is smallest, plus the term $\#C(\mathcal{Q}, \tilde{\mathcal{Q}})$ to ensure nesting of the resulting spline spaces. This third step is repeated until the sets $E(\tilde{\mathcal{Q}})$ and $C(\mathcal{Q}, \tilde{\mathcal{Q}})$ are empty.

2.3.2 Safe refinement for T-splines

Definition 2.20. For each level $k \in \mathbb{N}$, we define the tensor-product mesh

$$\mathcal{Q}_{k+1/2} := \left\{ [x - 2^{-k-1}, x] \times [y - 2^{-k}, y] \mid 2^{k+1}x \in \{1, \dots, 2^{k+1}M\}, 2^k y \in \{1, \dots, 2^k N\} \right\}.$$

Definition 2.21 (intermediate children). For $k \in \mathbb{N}_0$ and $q \in \mathcal{Q}_{k/2}$, we define

$$\text{SUBDIVIDE}^{1/2}(T) := \{T' \in \mathcal{Q}_{(k+1)/2} \mid T' \subset T\}.$$

Definition 2.22. The T-spline refinement procedure reads $\text{REFINE_TELEM}(\mathcal{Q}, \mathcal{M}) := (\mathcal{Q}_{\text{TSPLINE}}, \mathcal{B}_{\text{TSPLINE}})$, with

$$\begin{aligned} \tilde{\mathcal{Q}} &:= \mathcal{Q} \setminus \mathcal{M} \cup \text{SUBDIVIDE}^{1/2}(\mathcal{M}) \\ \text{and } \mathcal{B}_{\text{TSPLINE}}^{\tilde{\mathcal{Q}}} &:= \{B_v \mid v \in \mathcal{V}(\tilde{\mathcal{Q}})\}. \end{aligned}$$

Definition 2.23 (Safe refinement for T-splines). We define for each $q \in \mathcal{Q}$ the *coarse neighbourhood*

$$\mathcal{N}_{\text{TSPLINE}^{++}}(T) := \{T' \in \mathcal{Q} \cap \mathcal{Q}_{\ell(q)-1/2} \mid (\text{mid}(T) - \text{mid}(T')) \leq \mathbf{D}(\ell(q))\},$$

with

$$\mathbf{D}(k) = \begin{cases} 2^{-k/2} \left(\lfloor \frac{p}{2} \rfloor + \frac{1}{2}, \lfloor \frac{q}{2} \rfloor + \frac{1}{2} \right) & \text{if } k \text{ is even,} \\ 2^{-(k+1)/2} \left(\lceil \frac{p}{2} \rceil + \frac{1}{2}, 2 \lfloor \frac{q}{2} \rfloor + 1 \right) & \text{if } k \text{ is odd,} \end{cases}$$

where p and q are the polynomial degrees of the B-splines in x - and y -direction, respectively. Moreover, we define the *closure*

$$\text{CLOSURE_TSPLINE}^{++}(\mathcal{M}, \mathcal{Q}) := \bigcup_{k=0}^{\max \ell(\mathcal{M})} \mathcal{N}_{\text{TSPLINE}^{++}}^k(\mathcal{M}),$$

and the extended refinement procedure

$$\text{REFINE_TSPLINE}^{++}(\mathcal{Q}, \mathcal{M}) := \text{REFINE_TELEM}(\mathcal{Q}, \text{CLOSURE_TSPLINE}^{++}(\mathcal{M}, \mathcal{Q})).$$

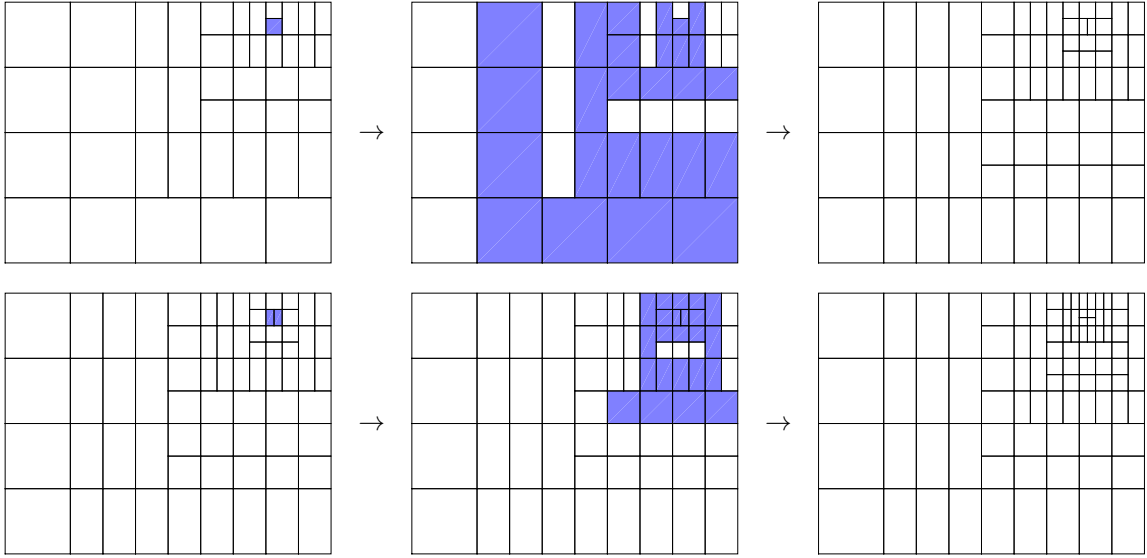


Figure 11: Example for the safe T-spline refinement. In order to subdivide the marked element as for the THB-spline refinement, the refinement routine $\text{REFINE_TSPLINE}^{++}$ is applied twice.

2.4 Theoretical Results

As mentioned in the introduction, the use of T-splines and local mesh refinement faces fundamental difficulties. Given a mesh $\mathcal{Q} \in \mathbb{M}_{\text{TSPLINE}}$ and a refinement \mathcal{Q}' of \mathcal{Q} , it is not clear in general that the T-spline functions that should serve as a spline basis are in fact linearly independent, and, even if they are, that the new spline space $\text{span } \mathcal{B}_{\text{TSPLINE}}^{\mathcal{Q}'}$ is a superspace of the preceding space $\text{span } \mathcal{B}_{\text{TSPLINE}}^{\mathcal{Q}}$. Both refinement procedures REFINE_TSPLINE^+ and $\text{REFINE_TSPLINE}^{++}$ overcome these problems.

Each of the refinement procedures $\text{REFINE} \in \{\text{REFINE_THB}^+, \text{REFINE_THB}^{++}, \text{REFINE_TSPLINE}^{++}\}$ satisfies the following properties [24, 8]:

- *Linear complexity.* There exists a constant C that depends only on the polynomial degree of the B-splines in use, such that any sequence of meshes $\mathcal{Q}_0, \mathcal{Q}_1, \dots, \mathcal{Q}_J$ with

$$\mathcal{Q}_j = \text{REFINE}(\mathcal{Q}_{j-1}, \mathcal{M}_{j-1}), \quad \mathcal{M}_{j-1} \subseteq \mathcal{Q}_{j-1} \quad \text{for } j \in \{1, \dots, J\}$$

satisfies

$$|\mathcal{Q}_J \setminus \mathcal{Q}_0| \leq C \sum_{j=0}^{J-1} |\mathcal{M}_j|.$$

This leads to linear complexity in terms of degrees of freedom. However, it does in general not reflect the complexity with respect to computing time or memory.

- *Bounded overlay.* For \mathcal{Q}_a and \mathcal{Q}_b being two meshes generated by \mathcal{Q}_0 and the successive use of REFINE, there exists a common refinement of $\hat{\mathcal{Q}}$ of \mathcal{Q}_a and \mathcal{Q}_b such that

$$\#\hat{\mathcal{Q}} + \#\mathcal{Q}_0 \leq \#\mathcal{Q}_a + \#\mathcal{Q}_b.$$

Moreover, each of these refinement procedures has a natural generalization to higher dimensions [14, 9], and due to the hierarchical construction of the mesh classes, they provably provide a stable shape regularity in the sense of bounded aspect ratios of the mesh elements and local quasi-uniformity of the mesh [8, Lemma 2.14]. Such analysis or higher-dimensional version is currently unavailable for REFINE_TSPLINE⁺.

3 Model Problems and Discretization

This section describes the two model problems that are used for our tests. We will formulate both problems in the weak (variational) form and skip their derivation from the original PDEs. The latter are, for the Poisson problem, seeking $u \in C^2(\bar{\Omega})$ such that

$$-\Delta u = f \text{ in } \Omega, \quad \frac{\partial u}{\partial \nu_N} = g \text{ on } \Gamma_N \quad \text{and} \quad u|_{\Gamma_D} = u_D \text{ on } \Gamma_D,$$

and for the problem of linear elasticity, seeking $u \in C^2(\bar{\Omega})$ such that

$$-\operatorname{div} \sigma(u) = f \text{ in } \Omega, \quad \langle \nu_N, \sigma(u) \rangle = g \text{ on } \Gamma_N \quad \text{and} \quad u|_{\Gamma_D} = u_D \text{ on } \Gamma_D,$$

using the notation explained below.

3.1 Poisson problem

Data Let $\Omega \subset \mathbb{R}^d$ be an open, connected and bounded Lipschitz domain. Let the Dirichlet boundary $\Gamma_D \subset \partial\Omega$ be closed and let each connectivity component of Γ_D be of positive measure. Set the Neumann boundary $\Gamma_N := \partial\Omega \setminus \Gamma_D$ and the corresponding outer normal vector $\nu_N : \Gamma_N \rightarrow \mathbb{R}^d$. Let $u_D \in L^2(\Gamma_D)$ and

$$H_0^1(\Omega) := \{w \in H^1(\Omega) \mid w|_{\Gamma_D} = 0 \text{ a.e. in } \Gamma_D\}.$$

Problem Find $u \in H^1(\Omega)$ such that

$$\begin{aligned} \int_{\Omega} \langle \nabla u, \nabla v \rangle dx &= \int_{\Omega} f v dx + \int_{\Gamma_N} g v ds \quad \text{for all } v \in H_0^1, \\ u|_{\Gamma_D} &= u_D \quad \text{a.e. on } \Gamma_D. \end{aligned} \tag{1}$$

Discretization Given a basis \mathcal{B} of a finite-dimensional function space $\hat{\mathcal{B}} := \operatorname{span} \mathcal{B}$ and

$$\hat{\mathcal{B}}_0 := \left\{ w \in \hat{\mathcal{B}} \mid w|_{\Gamma_D} = 0 \text{ a.e. in } \Gamma_D \right\},$$

we seek the Galerkin solution $\hat{u} \in \hat{\mathcal{B}}$ satisfying

$$\begin{aligned} \int_{\Omega} \langle \nabla \hat{u}, \nabla v \rangle dx &= \int_{\Omega} f v dx + \int_{\Gamma_N} g v ds \quad \text{for all } v \in \hat{\mathcal{B}}_0, \\ \hat{u}|_{\Gamma_D} &= I_{\hat{\mathcal{B}}}(u_D) \quad \text{on } \Gamma_D, \end{aligned} \tag{2}$$

where $I_{\hat{\mathcal{B}}}(u_D) \in \hat{\mathcal{B}}$ is an interpolation of u_D . We set $\hat{u}_0 := \hat{u} - I_{\hat{\mathcal{B}}}(u_D) \in \hat{\mathcal{B}}_0$ and reformulate the above problem to finding $\hat{u}_0 \in \hat{\mathcal{B}}_0$ such that

$$\int_{\Omega} \langle \nabla \hat{u}_0, \nabla v \rangle dx = \int_{\Omega} f v dx + \int_{\Gamma_N} g v ds - \int_{\Omega} \langle \nabla I_{\hat{\mathcal{B}}}(u_D), \nabla v \rangle dx \quad \text{for all } v \in \hat{\mathcal{B}}_0. \tag{3}$$

Since both left and right side of (2) are linear in v , it suffices to have the above equation fulfilled for all basis functions $v \in \mathcal{B}_0 = \{v_1, \dots, v_n\} = \mathcal{B} \cap \hat{\mathcal{B}}_0$ that are zero on the boundary. Since the right-hand side is also

linear in \hat{u}_0 , and $\hat{u}_0 \in \hat{\mathcal{B}}_0$ is a linear combination of these basis functions, (3) is equivalent to finding a vector $U = (u_1, \dots, u_n) \in \mathbb{R}^n$ such that

$$\underbrace{\left(\int_{\Omega} \langle \nabla v_i, \nabla v_j \rangle dx \right)_{1 \leq i, j \leq n}}_{A \in \mathbb{R}^{n \times n}} \cdot U = \underbrace{\left(\int_{\Omega} f v_i dx + \int_{\Gamma_N} g v_i ds - \int_{\Omega} \langle \nabla I_{\hat{\mathcal{B}}}(u_D), \nabla v_i \rangle dx \right)_{1 \leq i \leq n}}_{B \in \mathbb{R}^n}, \quad (4)$$

with $\hat{u} = \sum_{i=1}^n u_i v_i + I_{\hat{\mathcal{B}}}(u_D)$. We call A the *stiffness matrix* and B the *load vector*.

Error estimator The Adaptive Algorithm (explained below in Section 4) is controlled by a standard residual local error estimator $\eta : \mathcal{Q} \rightarrow \mathbb{R}$ (see e.g. [17] for an application with THB-splines). Given the Galerkin solution $\hat{u} \in \hat{\mathcal{B}}$, it is defined by

$$\eta_{\mathcal{Q}}(Q) := \left(h_Q^2 \|\Delta \hat{u} + f\|_Q^2 + \sum_{E \in \mathcal{E}(Q)} h_E \|R_E(\hat{u})\|_E^2 \right)^{1/2},$$

where $\mathcal{E}(Q)$ is the set of edges of Q , h_Q the diameter of Q , and h_E the length (the 1D Lebesgue measure) of the edge E . The notation $\|\bullet\|_A$ abbreviates the L^2 -norm $\|\bullet\|_{L^2(A)}$. The *edge residual* $R_E(\hat{u})$ is defined by

$$R_E(\hat{u}) := \begin{cases} \frac{1}{2} \llbracket \frac{\partial \hat{u}}{\partial \nu_E} \rrbracket_E & \text{if } E \text{ is an interior edge,} \\ g - \frac{\partial \hat{u}}{\partial \nu_E} & \text{if } E \text{ is a boundary edge.} \end{cases}$$

For any interior edge $E = Q \cap Q'$, the notation $\llbracket \bullet \rrbracket_E := \bullet|_Q - \bullet|_{Q'}$ describes the jump along the edge E . Note that in all four methods this paper accounts for, none of the spline basis functions have jumps in their derivatives, and the same holds for the discrete solution \hat{u} . Provided that the Neumann boundary condition is met exactly (e.g. in the case $g = 0$), the above error estimator hence reduces to

$$\eta_{\mathcal{Q}}(Q) := h_Q \|\Delta \hat{u} + f\|_Q.$$

3.2 Linear elasticity

Data Let Ω , Γ_D , Γ_N , ν_N , u_D as above. For $u \in H^1(\Omega, \mathbb{R}^d)$, we define

$$\varepsilon(u) := \left(\frac{1}{2} (\partial_i u_j + \partial_j u_i) \right)_{1 \leq i, j \leq d} \quad \text{and} \quad \sigma(u)_{ij} := \sum_{1 \leq k, \ell \leq d} C_{ijkl} \varepsilon(u)_{kl} \quad \text{for } 1 \leq i, j \leq d.$$

We call u the *displacement*, $\varepsilon(u)$ the *strain tensor* and $\sigma(u)$ the *stress tensor*, and C is some positive definite fourth order tensor that describes material properties.

Problem Find $u \in H^1(\Omega)$ such that

$$\begin{aligned} \int_{\Omega} \langle \sigma(u), \varepsilon(v) \rangle dx &= \int_{\Omega} f v dx + \int_{\Gamma_N} g v ds \quad \text{for all } v \in H_0^1(\mathbb{R}^d), \\ u|_{\Gamma_D} &= u_D \quad \text{a.e. on } \Gamma_D. \end{aligned} \quad (5)$$

Discretization Given a basis \mathcal{B} of a finite-dimensional function space $\hat{\mathcal{B}} := \text{span } \mathcal{B}$ and $\hat{\mathcal{B}}_0$ as above, we seek the Galerkin solution $\hat{u} \in \hat{\mathcal{B}}$ satisfying

$$\begin{aligned} \int_{\Omega} \langle \sigma(\hat{u}), \varepsilon(v) \rangle dx &= \int_{\Omega} f v dx + \int_{\Gamma_N} g v ds \quad \text{for all } v \in \hat{\mathcal{B}}_0, \\ \hat{u}|_{\Gamma_D} &= I_{\hat{\mathcal{B}}}(u_D) \quad \text{on } \Gamma_D. \end{aligned} \quad (6)$$

Again, we set $\hat{u}_0 := \hat{u} - I_{\hat{\mathcal{B}}}(u_D) \in \hat{\mathcal{B}}_0$ and reformulate the above problem to finding $\hat{u}_0 \in \hat{\mathcal{B}}_0$ such that

$$\int_{\Omega} \langle \sigma(\hat{u}_0), \varepsilon(v) \rangle dx = \int_{\Omega} f v dx + \int_{\Gamma_N} g v ds - \int_{\Omega} \langle \sigma(I_{\hat{\mathcal{B}}}(u_D)), \varepsilon(v) \rangle dx \quad \text{for all } v \in \hat{\mathcal{B}}_0. \quad (7)$$

Analogously to the derivation for the Poisson problem above, we compute the Galerkin solution by solving the equation

$$\underbrace{\left(\int_{\Omega} \langle \sigma(v_i), \varepsilon(v_j) \rangle dx \right)_{1 \leq i, j \leq n}}_{A \in \mathbb{R}^{n \times n}} \cdot U = \underbrace{\left(\int_{\Omega} f v_i dx + \int_{\Gamma_N} g v_i ds - \int_{\Omega} \langle \sigma(I_{\hat{\mathcal{B}}}(u_D)), \varepsilon(v_i) \rangle dx \right)_{1 \leq i \leq n}}_{B \in \mathbb{R}^n}. \quad (8)$$

and setting $\hat{u} = \sum_{i=1}^n u_i v_i + I_{\hat{\mathcal{B}}}(u_D)$.

Error estimator Given the Galerkin solution $\hat{u} \in \hat{\mathcal{B}}$, we use the local error estimator described in [29], which is defined by

$$\eta_{\mathcal{Q}}(\mathcal{Q}) := \left(h_{\mathcal{Q}}^2 \|\operatorname{div} \sigma(\hat{u}) + f\|_{\mathcal{Q}}^2 + \sum_{E \in \mathcal{E}(\mathcal{Q})} h_E \|R_E(\hat{u})\|_E^2 \right)^{1/2},$$

where the *edge residual* $R_E(\hat{u})$ is defined by

$$R_E(\hat{u}) := \begin{cases} \frac{1}{2} \llbracket \langle \nu_E, \sigma(\hat{u}) \rangle \rrbracket_E & \text{if } E \text{ is an interior edge,} \\ g - \langle \nu_E, \sigma(\hat{u}) \rangle & \text{if } E \text{ is a boundary edge.} \end{cases}$$

4 Adaptive Algorithm

4.1 Adaptive Loop

The Adaptive Algorithm is an iterative procedure that consist of the steps



which are described as follows.

SOLVE: Given a finite-dimensional function space, compute a Galerkin approximation of the solution of the PDE.

ESTIMATE: Compute local estimates for the error, i.e., the difference of approximate and exact solution.

MARK: Based on these local estimates, select mesh elements $\mathcal{M} \subseteq \mathcal{Q}$ for refinement.

REFINE: Refine the mesh \mathcal{Q} and construct the new discrete function space \mathcal{B} .

Due to their dependence on the particular problem, the modules **SOLVE** and **ESTIMATE** have been defined above, for the two problems considered. For the module **REFINE**, we consider four variants, which have been outlined in Section 2.

4.2 Marking Strategies

Given the estimated local errors $\{\eta_{\mathcal{Q}} \mid \mathcal{Q} \in \mathcal{Q}\} \subset \mathbb{R}$ and a marking parameter $\theta \in [0, 1]$, which is chosen manually, the following strategies are commonly used for the step **MARK**.

- *Quantile marking:* Let $\mathcal{Q} = \{\mathcal{Q}_1, \dots, \mathcal{Q}_K\}$ and $\eta_{\mathcal{Q}}(\mathcal{Q}_1) \geq \dots \geq \eta_{\mathcal{Q}}(\mathcal{Q}_K)$, then $\mathcal{M} = \{\mathcal{Q}_1, \dots, \mathcal{Q}_k\}$ with $k \approx \theta K$.
- *Dörfler marking:* Let $\mathcal{Q} = \{\mathcal{Q}_1, \dots, \mathcal{Q}_K\}$ and $\eta_{\mathcal{Q}}(\mathcal{Q}_1) \geq \dots \geq \eta_{\mathcal{Q}}(\mathcal{Q}_K)$, then $\mathcal{M} = \{\mathcal{Q}_1, \dots, \mathcal{Q}_k\}$ with

$$\sum_{j=1}^{k-1} \eta_{\mathcal{Q}}(\mathcal{Q}_j) < \theta \sum_{\mathcal{Q} \in \mathcal{Q}} \eta_{\mathcal{Q}}(\mathcal{Q}) \quad \text{and} \quad \sum_{j=1}^k \eta_{\mathcal{Q}}(\mathcal{Q}_j) \geq \theta \sum_{\mathcal{Q} \in \mathcal{Q}} \eta_{\mathcal{Q}}(\mathcal{Q}).$$

- *Maximum marking:* $\mathcal{M} := \{\mathcal{Q} \in \mathcal{Q} \mid \eta_{\mathcal{Q}}(\mathcal{Q}) \geq \theta \max_{\tilde{\mathcal{Q}} \in \mathcal{Q}} \eta_{\mathcal{Q}}(\tilde{\mathcal{Q}})\}$.

4.3 Optimality of the Adaptive Algorithm

In the case of Quantile marking, the authors are not aware of theoretical results that ensure optimality of the convergence rates. If the Adaptive FEM is applied with Dörfler marking, the sequence of discrete solutions $u_1 \in \hat{\mathcal{B}}_1 \in \mathbb{B}$, $u_2 \in \hat{\mathcal{B}}_2 \in \mathbb{B}$, ... has the best convergence rate (w.r.t. degrees of freedom) that is possible in the class \mathbb{B} of discrete function spaces [30, 31, 32, 25]. For a modified version of Maximum marking, the discrete solutions are proven to be instance-optimal [33]. This means that in each step, the error of the discrete solution $u \in \hat{\mathcal{B}} \in \mathbb{B}$ is bounded by a constant times the smallest error of the discrete solutions of all function spaces $\hat{\mathcal{B}}' \in \mathbb{B}$ with a comparable (or smaller) number of degrees of freedom. This is an even stronger result than the rate optimality described above, however [33] accounts only for the Poisson problem with homogeneous Dirichlet boundary condition, i.e., $\Gamma_N = \emptyset$ and $u_D = 0$, and the authors are only aware of a generalization for the nonconforming Crouzeix-Raviart AFEM and the Stokes equation [34].

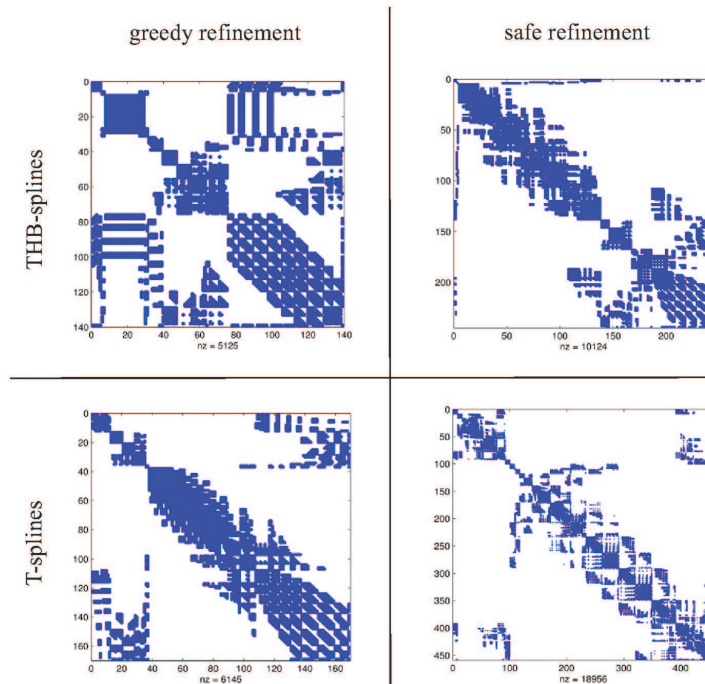


Figure 12: Worst case scenario: The sparsity patterns of the stiffness matrices after six refinement steps are illustrated. Especially the greedy THB-spline refinement results in a dense stiffness matrix.

5 Numerical Experiments

In this section, the mesh refinement strategies from Section 2 are compared numerically. Hence, T-splines are compared with THB-splines and greedy with safe refinement. In addition to achievable convergence rates and the mesh grading, the comparison includes the numerical properties of the stiffness matrix as its sparsity and condition number. To clearly point out differences between the refinement strategies, the first example is designed as a worst case scenario and does not correspond to a physical problem. The second and third example are well-established benchmark problems in the context Adaptive Finite Element Methods [2, 12, 27], including the Poisson problem and linear elasticity with given analytical solutions. In all examples and for all refinement strategies, cubic B-spline basis functions are used.

5.1 Worst case scenario

In this example, an initial square mesh with 64 elements is locally refined in the lower left corner, where only one element is marked for refinement in each refinement loop. The resulting Bézier meshes are presented in Figure 1. It can be seen that the greedy THB-spline refinement does only refine the marked element whereas the safe refinement routines extend the refinement region. Also the greedy T-spline refinement has to insert additional control points to ensure analysis-suitability. The total number of degrees of freedom (DOF) is plotted against the refinement steps in Figure 13 (a) to illustrate this behaviour.

The locality of the refinement comes at the cost of an increased interaction between differently scaled basis functions (cf. Section 2.2) in the case of greedy THB-spline refinement. In this example, basis functions from the coarsest level interact with basis functions of the finest level. This leads to the occurrence of quasi-dense rows and columns and the loss of any band structure in the stiffness matrix, as it can be seen in Figure 12. The other refinement routines do not produce anomalies in their sparsity patterns.

The local mesh refinement also influences the behaviour of the condition number of the stiffness matrix. Galhaut et al. [35] analyzed these condition numbers for NURBS-based isogeometric discretizations, showing that the condition number increases linearly with respect to degrees of freedom. This is also reflected in all our experiments. As expected, we observe for all kinds of local refinement that the condition numbers grow at higher rates, see Figure 13 (b). The rate is apparently independent of the type (T- or THB-splines) but does depend on the locality of refinement (greedy or safe), and thus on the grading of the mesh. However, if the condition numbers are compared with respect to the refinement step (cf. Figure 13 (c)), the safe THB-spline refinement produces higher condition numbers than the greedy one, and the T-splines higher condition numbers than the THB-splines. This shows that the number of additional DOF per refinement step can have a dominant influence on the condition

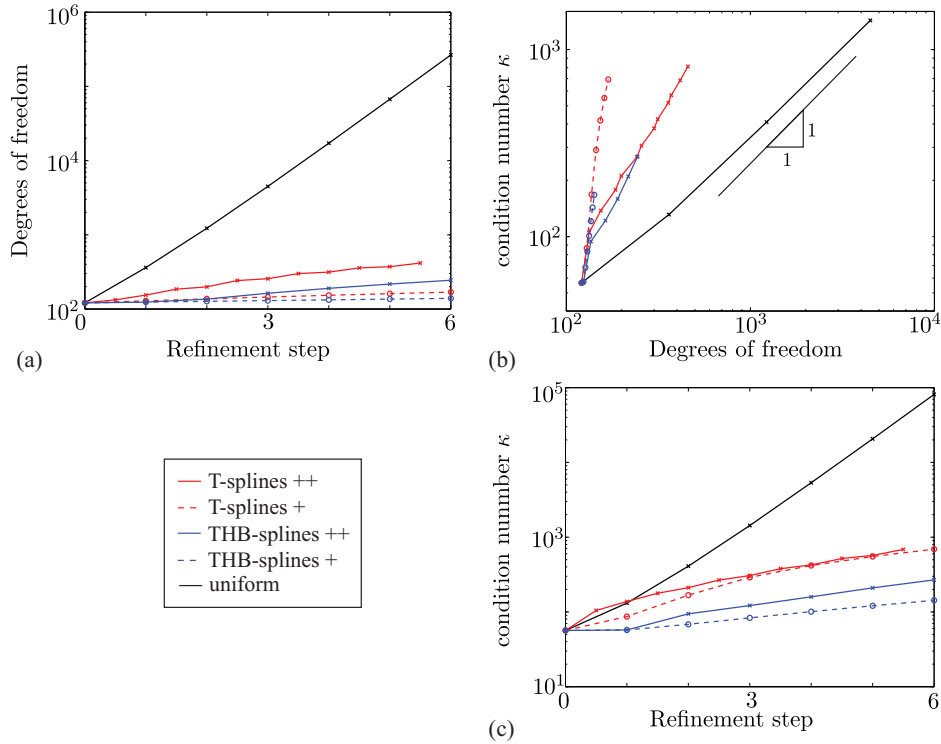


Figure 13: Worst case scenario: The relations between the total number of degrees of freedom, the condition number of the stiffness matrix and the refinement steps are illustrated.

number. Hence, for a clear comparison, the condition number has to be compared with respect to a quantity of main interest. For this reason the numerical error of the solution will be plotted over the condition number in the following examples. We emphasize that this discussion disregards appropriate preconditioning, but is beyond the scope of this paper.

5.2 Poisson problem

In this example, the Poisson problem (cf. Section 3.1) is solved for the temperature u on two different two-dimensional domains. The first domain $\Omega_L = \{(-1, 1) \times (-1, 1)\} \setminus \{(0, 1) \times (0, 1)\}$, referred to as the L-Shape, is characterized by a re-entrant corner with an opening angle of $\beta = 90^\circ$ and a given exact solution

$$\bar{u} = r^{\frac{2}{3}} \sin \frac{2\phi - \pi}{3} \quad (9)$$

in polar coordinates (r, ϕ) . The second domain $\Omega_S = \{(-1, 1) \times (-1, 1)\}$, referred to as the slit domain, is characterized by a re-entrant corner with an opening angle of $\beta = 0^\circ$ and a given exact solution

$$\bar{u} = r^{\frac{1}{2}} \sin \frac{\phi}{2}. \quad (10)$$

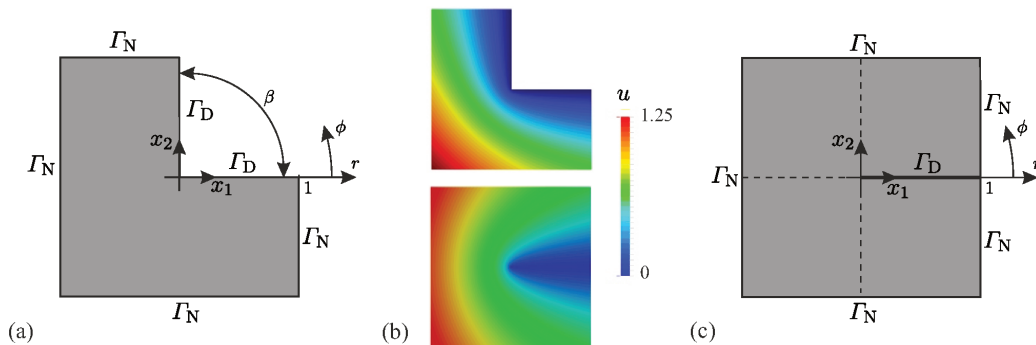


Figure 14: Poisson problem: Domain and boundary conditions for (a) the L-shape and (c) the slit domain as well as (b) the corresponding analytical solutions.

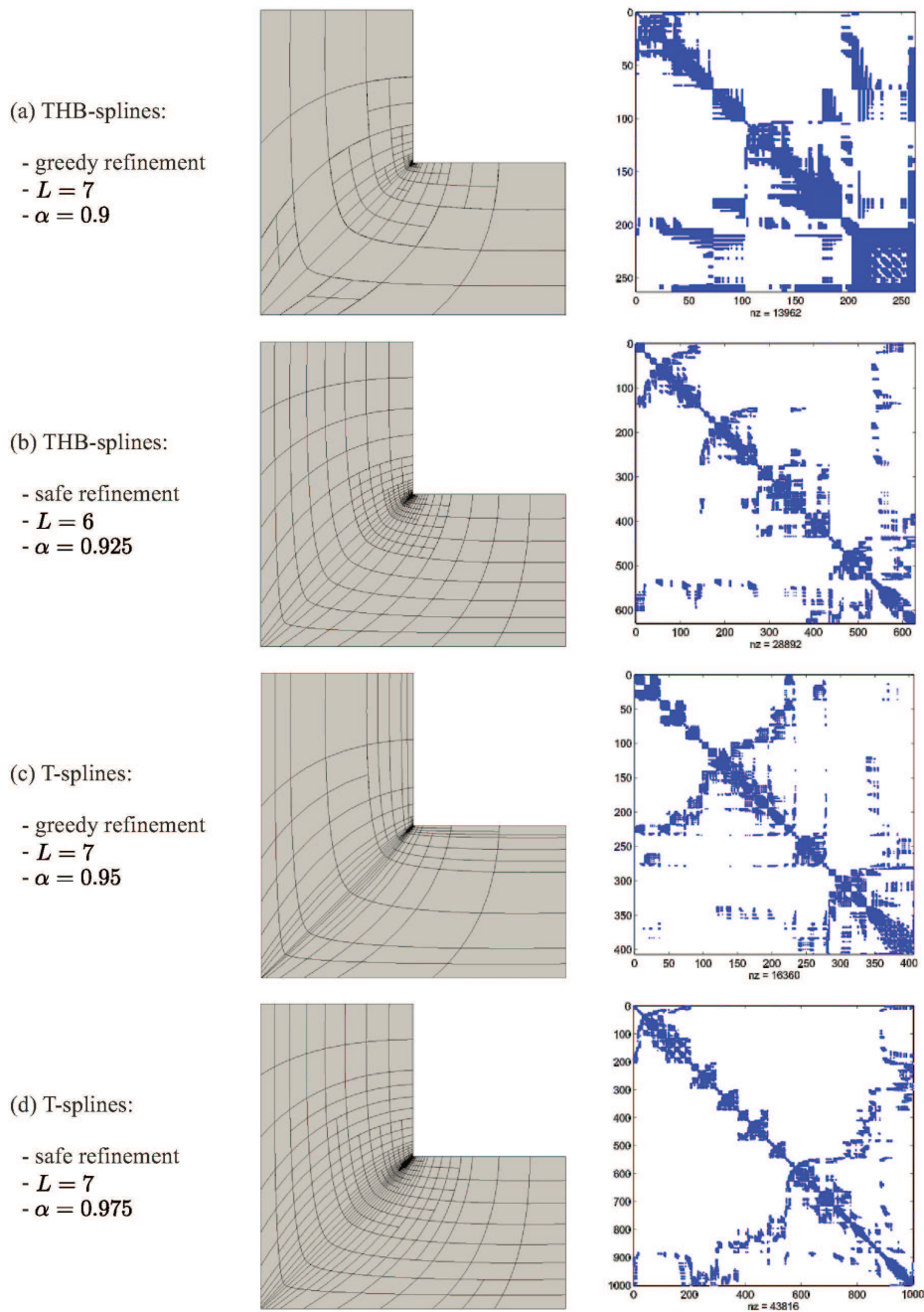


Figure 15: L-shape: The marking parameters α , the Bézier meshes and the sparsity patterns of the stiffness matrices after L refinement steps for all (a)-(d) refinement strategies. The safe refinement strategies result in well graded meshes, the greedy refinement strategies in more unstructured meshes. Again, the greedy THB-spline refinement creates the stiffness matrix with the highest density and interaction.

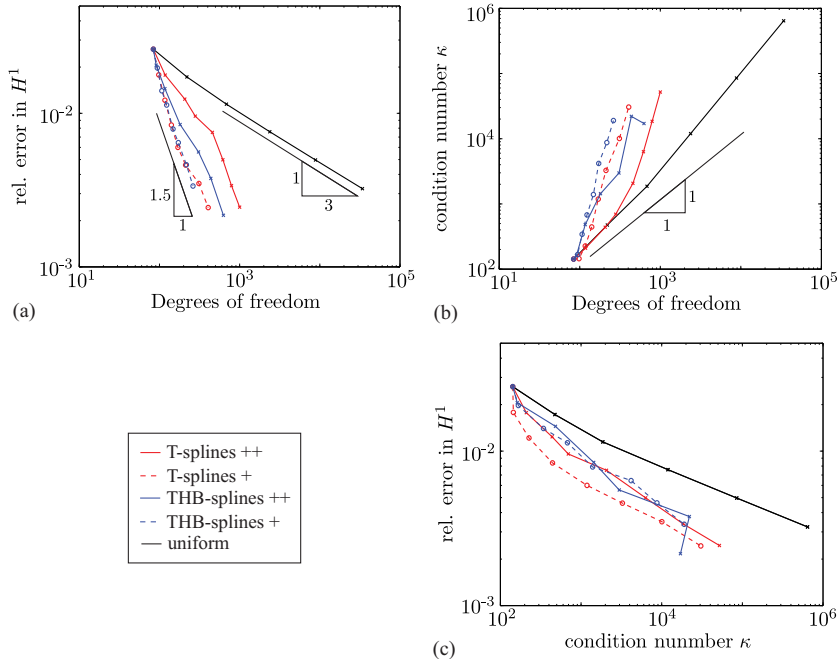


Figure 16: L-shape: The convergence rates as well as the relations between the condition number of the stiffness matrix, the numerical error of the solution and the total number of degrees of freedom are illustrated. **(a)** - All refinement strategies converge with the expected convergence rate $k = 1.5$ in the asymptotic range.

Both boundary value problems are illustrated in Figure 14. The boundary conditions are applied by setting $u = 0$ at the Dirichlet boundary Γ_D and the exact heat flux $g = \partial \bar{u} / \partial \nu_N$ at the Neumann boundary Γ_N . The L-Shape is modelled by a single C^1 -continuous B-spline patch, while the slit domain is modelled by a single B-spline patch with C^0 -continuous lines at the axis of symmetry of the domain as indicated by the dashed lines in Figure 14.

In both problems, the geometry leads to a singularity of the solution at the re-entrant corner. In this case classical convergence theory does not hold, and the order of convergence with respect to the total number of degrees of freedom

$$k = -\frac{1}{2} \min\left(p, \frac{\pi}{2\pi - \beta}\right) \quad (11)$$

is governed by the angle β of the re-entrant corner [36]. For uniform h -refinement this leads to a convergence rate of $k = -1/3 \forall p$ for the L-shape and $k = -1/4 \forall p$ for the slit domain.

The optimal order of convergence $k = -p/2$ can be recovered by local mesh refinement in the vicinity of the singularity. In the following, the adaptive finite element method (cf. Section 4) will be applied to solve the problem above with different refinement strategies. To select elements for refinement, the quantile marking (cf. Section 4.2) is used. The associated parameter α is adjusted for each refinement strategy, to achieve best possible convergence rates.

5.2.1 L-Shape

The initial mesh of the L-shape problem consists of 16 elements. Figure 15 shows the Bézier meshes after L refinement steps, as well as the marking parameters α . For the adaptive local refinement, the error in the H^1 norm is plotted over the total number of degrees of freedom (DOF) in Figure 16 (a). All refinement strategies recover the optimal order of convergence in the asymptotic range. Due to the coarse initial mesh, the safe refinements produce a greater amount of DOF in the pre-asymptotic range which is in particular observed for the safe T-spline refinement. As a result, the safe refinements are not as local as the greedy refinements but create more smoothly graded meshes. To counteract the non-local refinements, the marking parameter for safe refinements is chosen higher.

Especially for the greedy THB-spline refinement, the computed stiffness matrix has a higher density. For all other refinement strategies no clear tendency is visible in the sparsity patterns in Figure 15.

The condition number is plotted over the DOF in Figure 16 (b). Due to the geometric map of the L-shape, a rate higher than one is reached for uniform refinement. Regarding the local refinement, results similar to the

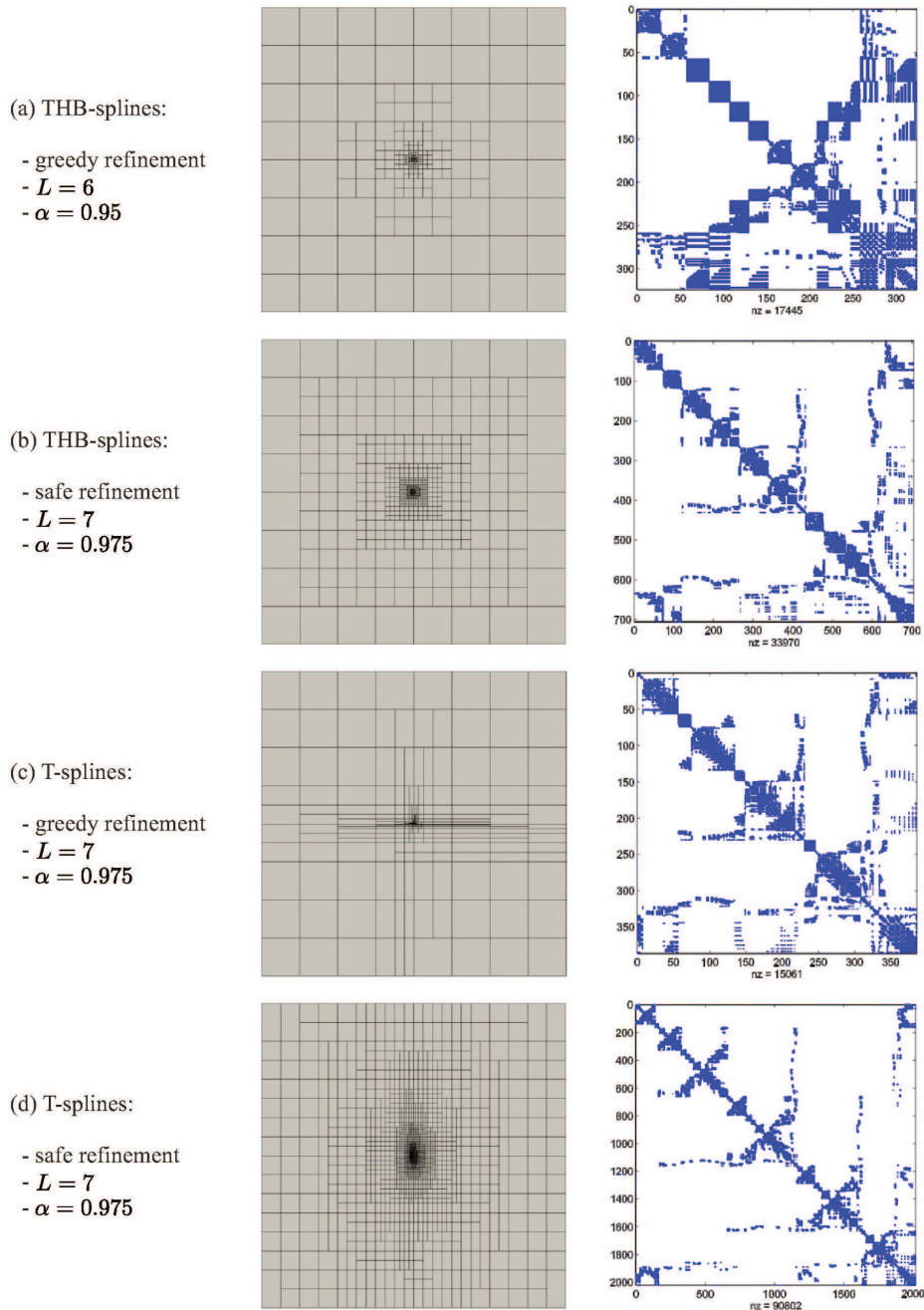


Figure 17: Slit domain: The marking parameters α , the Bézier meshes and the sparsity patterns of the stiffness matrices after L refinement steps for all (a)-(d) refinement strategies. The safe refinement strategies result in well graded meshes. Especially the greedy T-spline refinement creates an unstructured mesh with badly shaped elements. Again, the greedy THB-spline refinement creates the stiffness matrix with the highest density and interaction.

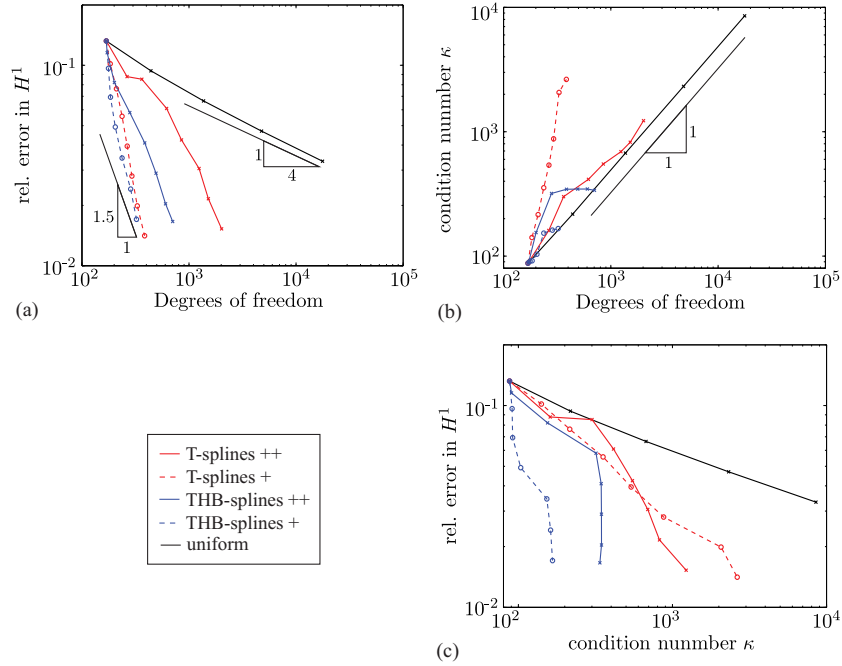


Figure 18: Slit domain: The convergence rates as well as the relations between the condition number of the stiffness matrix, the numerical error of the solution and the total number of degrees of freedom are illustrated. **(a)** - All refinement strategies converge with the expected convergence rate $k = 1.5$ in the asymptotic range.

previous example are obtained. However, the differences between the greedy and safe refinements are not as large as in the first experiment.

As mentioned above, also the error of the numerical solution with respect to the condition number (cf. Figure 16 (c)) is of interest. It can be seen that for the same order of accuracy, all local refinement techniques produce smaller condition numbers compared to the uniform case. This means, that for local refinement, the error of the solution decreases faster per DOF than the condition number increases per DOF. This is an important result, because it illustrates that the negative influence of a locally refined mesh on the condition number does not predominate the benefits of local refinement regarding the error level. The refinement strategies compared among themselves show similar results.

5.2.2 Slit domain

The initial mesh of the slit domain consists of 64 elements. The Bézier meshes after L refinement steps, as well as the marking parameters α are illustrated in Figure 17. As expected, the meshes of the safe refinement routines propagate the refinement area but produce well graded meshes. On the other hand, the greedy T-spline refinement leads to a mesh with little structure and badly shaped elements with aspect ratios up to 64. Concerning the sparsity patterns of the stiffness matrix, only the greedy THB-spline refinement creates matrices with a higher density, due to the increased interaction between the basis functions.

For the adaptive local refinement, the error in the H^1 norm is plotted over the total number of degrees of freedom (DOF) in Figure 18 (a). It can be seen that the error of the greedy refinement routines appear to converge with a higher rate in the pre-asymptotic range and later approach the theoretically predicted rate of $k = 1.5$. The safe refinement routines have a minor convergence rate in the pre-asymptotic range, but then also converge with the theoretical rate of $k = 1.5$. A reason for this behaviour can be found again in the relatively coarse initial mesh, which forces the safe T-spline refinement to refine almost the whole domain in the first refinement steps. As a result, the safe T-spline refinement requires six times more degrees of freedom than the greedy T-spline refinement for the same error level.

The condition number is plotted over the DOF in Figure 18 (b). Due to the badly shaped elements, the condition number for the greedy T-spline refinement increases fastest. The THB-spline refinements instead seem to benefit from their hierarchical structure together with the absence of a deforming geometry mapping. At a certain stage of refinement, the condition number does not increase further. This behaviour has been also found in [15] where HB-splines are compared against THB- and L-RB-splines. In the context of hierarchical Finite Elements [37], it is known and even proven that the condition number of the stiffness matrix scales with $O(\log(\text{DOF}))$ instead of

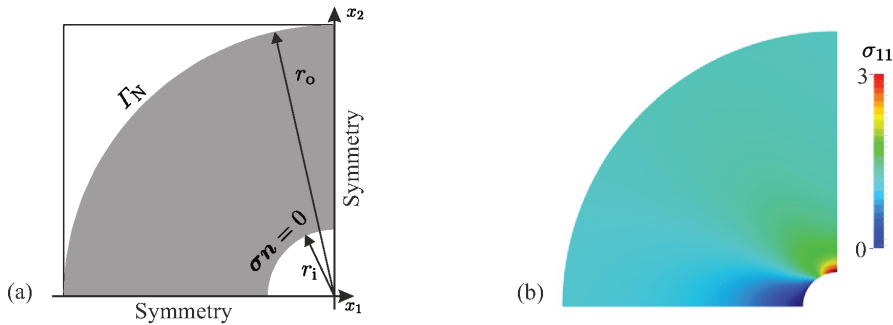


Figure 19: Infinite plate with a circular hole: (a) numerical analysis domain and boundary conditions, and (b) solution for σ_{11} .

$O(\text{DOF})$, due to orthogonalities w.r.t. to the energy product between basis functions of different levels. In 1D, this leads to block-diagonal stiffness matrices; in higher dimensions, this effect is milder (see e.g. Figure 17 (a)), but still yields good conditioning. It seems that (Truncated) Hierarchical B-splines share these benefits, however further investigation is needed in future.

Due to this effect, the greedy THB-spline refinement performs best if the numerical error is plotted over the condition number (cf. Figure 18 (c)). Since only a small amount of DOF is added during the refinement and due to the fact that the condition number grows slowly per DOF, an increased level of accuracy can be reached without increasing the condition number. But compared to the uniform refinement, also the T-spline refinements produce smaller condition numbers.

5.3 Linear elasticity

As a third example, an infinite plate with a circular hole under uniaxial in-plane tension σ_0 according to Figure 19 (a) is considered. The analytical solution is given by Timoshenko [38] in polar coordinates (r, ϕ)

$$\bar{\sigma}_r = \frac{\sigma_0}{2} \left[1 - \frac{r_i^2}{r^2} + \left(1 - 4\frac{r_i^2}{r^2} + 3\frac{r_i^4}{r^4} \right) \cos(2\phi) \right] \quad (12)$$

$$\bar{\sigma}_\phi = \frac{\sigma_0}{2} \left[1 + \frac{r_i^2}{r^2} - \left(1 + 3\frac{r_i^4}{r^4} \right) \cos(2\phi) \right] \quad (13)$$

$$\bar{\sigma}_{r\phi} = \frac{\sigma_0}{2} \left(-1 - 2\frac{r_i^2}{r^2} + 3\frac{r_i^4}{r^4} \right) \sin(2\phi) \quad (14)$$

where $r_i = 1 \text{ mm}$ is the radius of the hole. A numerical solution is conveniently obtained on the quarter of an annulus with Dirichlet boundaries to enforce the symmetry conditions, and a Neumann boundary Γ_N at the outer radius to enforce the exact normal stress. The uniaxial tensile stress $\sigma_0 = 1 \text{ MPa}$ is applied in the x_1 -direction and material parameters $E = 10^5 \text{ Pa}$ and $\nu = 0.3$ are used. The computational domain is modelled by a single C^1 -continuous NURBS patch with an outer radius $r_o = 8$.

The exact solution features a stress concentration at $(x, y) = (0, r_i)$ of $\sigma_{11} = 3\sigma_0$ as illustrated in Figure 19 (b). Due to the lack of a singularity, optimal convergence rates $k = -p/2$ can be obtained by uniform h -refinement. Local refinement does not improve this rate in the asymptotic limit [2, 12]. There is however a benefit of the adaptive refinement which increases with the locality of the stress concentration. That is, if the outer radius r_o is larger, the stress concentration is more localised in the computational domain, cf. Figure 20 (a), and an improved convergence rate can be achieved in the pre-asymptotic region.

This improvement can be obtained for all refinement techniques by setting the marking parameter around $\alpha = 0.5$ to generate a more extensive refinement. For this example the greedy and safe THB-spline refinement produce same results. The meshes after L refinement steps and the marking parameters α are illustrated in Figure 20. All refinement techniques lead to similar meshes. As a result, also the sparsity patterns are quiet similar and do not show any tendency. If the condition number is plotted over DOF (cf. Figure 21 (b)), no differences in the rate are visible between local and uniform refinement. In general it may be said that no numerical differences occur between the refinement techniques if the refinement area is extensive.

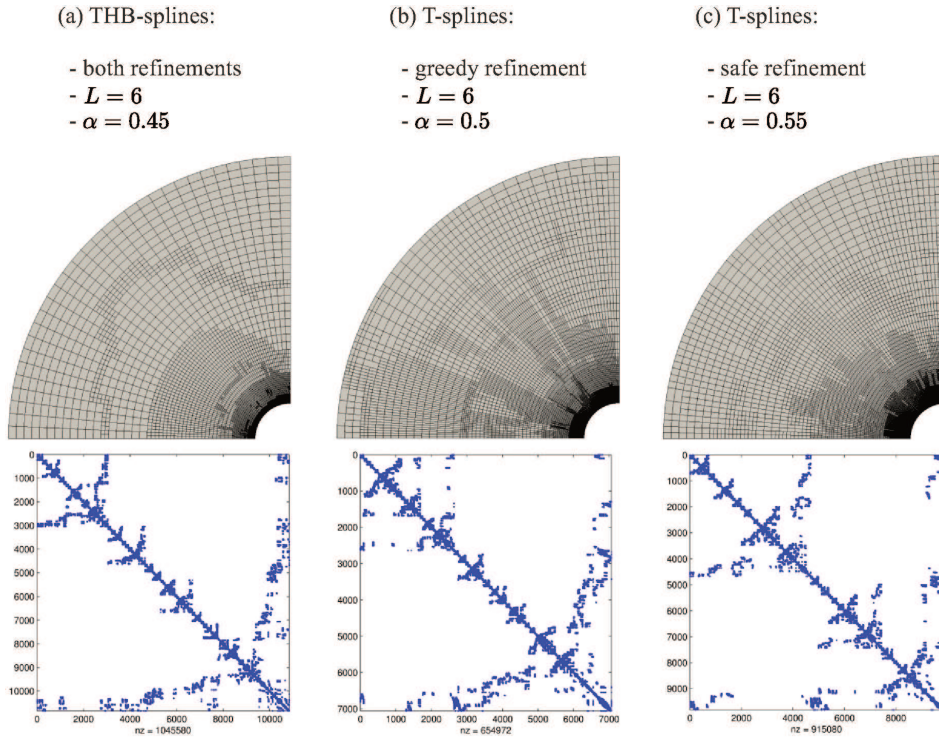


Figure 20: Infinite plate with a circular hole: The marking parameters α , the Bézier meshes and the sparsity patterns of the stiffness matrices after L refinement steps for all (a)-(d) refinement strategies. The greedy and safe THB-spline refinement show an identical refinement behaviour. Neither in the Bézier meshes, nor in the sparsity patterns, clear differences between the refinement strategies are visible.

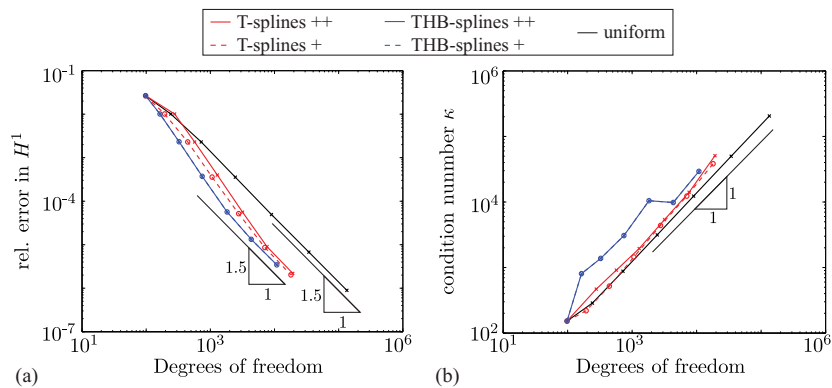


Figure 21: Infinite plate with a circular hole: The convergence rates as well as the condition number over the total number of degrees of freedom is plotted. (a) - The local refinement strategies improve the convergence rate in the pre-asymptotic regime, but reduce to $k = 1.5$ in the asymptotic region.

6 Conclusions

In this contribution, four different refinement techniques based on T- and THB-splines have been applied to the Adaptive Finite Element Method and compared regarding their theoretical and numerical properties. For this purpose, four numerical examples have been studied.

In general, the successive use of an elementary refinement routine such as `REFINE_THB` or `REFINE_TELEM` causes uncontrolled function overlap and dense stiffness matrices in the case of THB-splines, or yields non-nested discrete spaces in the case of T-splines (which means for an isogeometric method that the geometry is not preserved), or does not even yield an actual basis due to linear dependencies (also for T-splines).

The refinement routine `REFINE_TSPLINE+` eliminates these major drawbacks from a practical approach, yielding an efficient and flexible refinement routine. The procedure `REFINE_THB+` is a practical approach to avoid the above-mentioned dense stiffness matrices, which is only partially achieved. On the other hand, it satisfies the same theoretical properties (namely linear complexity and bounded overlay) as the safe refinement routines, while such analysis for `REFINE_TSPLINE+` is currently not available.

The safe refinement routines `REFINE_THB++` and `REFINE_TSPLINE++` have shown the expected optimal asymptotical behavior that has been predicted in theory, however they did not outperform the greedy refinement routines in our experiments.

Concerning the mesh grading and the numerical properties of the stiffness matrix, obvious differences increase with the locality of the problem. The refinement routines behave similar for extensive refinements, but differ the more local the refinement area is selected. For these local refinement areas, the greedy refinement routines show a clear increase in the condition number per degree of freedom and especially for the refinement routine `REFINE_THB+` dense stiffness matrices arise. Furthermore, the greedy refinement routines lead to unstructured meshes around the refinement area. For the refinement routine `REFINE_TSPLINE+` this can lead to badly shaped elements with ever-growing aspect ratios (in our experiments, up to 64).

From the implementation point of view, which is only a subjective view of the authors, the implementation effort increases from the refinement routine `REFINE_THB+` to `REFINE_THB++` to `REFINE_TSPLINE++` to `REFINE_TSPLINE+`. The effort grows further for T-splines in general if a polynomial degree distinct from three is used, or for the greedy T-spline refinement, if a generalisation to three dimension is desired.

References

- [1] Y. Bazilevs, V. M. Calo, J. A. Cottrell, J. Evans, T. J. R. Hughes, S. Lipton, M. A. Scott, T. W. Sederberg, Isogeometric analysis using T-splines, *Computer Methods in Applied Mechanics and Engineering* 199 (2010) 229–263.
- [2] M. R. Dörfel, B. Jüttler, B. Simeon, Adaptive isogeometric analysis by local h-refinement with T-splines, *Computer Methods in Applied Mechanics and Engineering* 199 (2010) 264–275.
- [3] A. Buffa, D. Cho, G. Sangalli, Linear independence of the T-spline blending functions associated with some particular T-meshes, *Computer Methods in Applied Mechanics and Engineering* 199 (23–24) (2010) 1437 – 1445. doi:10.1016/j.cma.2009.12.004.
- [4] L. B. da Veiga, A. Buffa, D. Cho, G. Sangalli, Analysis-suitable T-splines are dual-compatible, *Computer Methods in Applied Mechanics and Engineering* 249–252 (2012) 42 – 51, Higher Order Finite Element and Isogeometric Methods. doi:10.1016/j.cma.2012.02.025.
- [5] X. Li, J. Zheng, T. W. Sederberg, T. J. Hughes, M. A. Scott, On linear independence of T-spline blending functions, *Computer Aided Geometric Design* 29 (1) (2012) 63 – 76, geometric Constraints and Reasoning. doi:10.1016/j.cagd.2011.08.005.
- [6] M. Scott, X. Li, T. Sederberg, T. Hughes, Local refinement of analysis-suitable T-splines, *Computer Methods in Applied Mechanics and Engineering* 213–216 (2012) 206 – 222. doi:10.1016/j.cma.2011.11.022.
- [7] X. Li, M. A. Scott, Analysis-suitable T-splines: Characterization, refineability, and approximation, *Mathematical Models and Methods in Applied Sciences* 24 (06) (2014) 1141–1164. doi:10.1142/S0218202513500796.
- [8] P. Morgenstern, D. Peterseim, Analysis-suitable adaptive T-mesh refinement with linear complexity, *Comput. Aided Geom. Design* 34 (0) (2015) 50–66. doi:10.1016/j.cagd.2015.02.003.
- [9] P. Morgenstern, 3D Analysis-suitable T-splines: definition, linear independence and m-graded local refinement, arXiv e-prints. Submitted for publication. arXiv:1505.05392.

- [10] D. R. Forsey, R. H. Bartels, Hierarchical B-spline refinement, *Computer Graphics* 22 (1988) 205–212.
- [11] R. Kraft, Adaptive and linearly independent multilevel B-splines, in: A. Le Méhauté, C. Rabut, L. L. Schumaker (Eds.), *Surface Fitting and Multiresolution Methods*, Vanderbilt University Press, Nashville, 1997, pp. 209–218.
- [12] A.-V. Vuong, C. Giannelli, B. Jüttler, B. Simeon, A hierarchical approach to adaptive local refinement in isogeometric analysis, *Comput. Methods Appl. Mech. Engrg.* 200 (49-52) (2011) 3554–3567.
- [13] G. Kuru, C. V. Verhoosel, K. G. van der Zee, E. H. van Brummelen, Goal-adaptive isogeometric analysis with hierarchical splines, *Computer Methods in Applied Mechanics and Engineering* 270 (2014) 270–292.
- [14] C. Giannelli, B. Jüttler, H. Speleers, THB-splines: the truncated basis for hierarchical splines, *Computer Aided Geometric Design* 29 (2012) 485–498.
- [15] K. A. Johannessen, F. Remonato, T. Kvamsdal, On the similarities and differences between Classical Hierarchical, Truncated Hierarchical and LR B-splines, *Comput. Methods Appl. Mech. Engrg.* 291 (2015) 64–101.
- [16] D. Schillinger, L. Dede, M. A. Scott, J. A. Evans, M. J. Borden, E. Rank, T. J. R. Hughes, An isogeometric design-through-analysis methodology based on adaptive hierarchical refinement of NURBS, immersed boundary methods, and T-spline CAD surfaces, *Comput. Methods Appl. Mech. Engrg.* 249 (2012) 116–150.
- [17] A. Buffa, C. Giannelli, Adaptive isogeometric methods with hierarchical splines: error estimator and convergence, *Archiv e-prints* (2015).
- [18] T. Dokken, T. Lyche, K. F. Pettersen, Polynomial splines over locally refined box-partitions, *Computer Aided Geometric Design* 30 (2013) 331–356.
- [19] A. Bressan, Some properties of LR-splines, *Computer Aided Geometric Design* 30 (2013) 778–794.
- [20] E. Evans, M. Scott, X. Li, D. Thomas, Hierarchical T-splines: Analysis-suitability, Bézier extraction, and application as an adaptive basis for isogeometric analysis, *Computer Methods in Applied Mechanics and Engineering* 284 (0) (2015) 1–20, isogeometric Analysis Special Issue. doi:10.1016/j.cma.2014.05.019.
- [21] H. Kang, F. Chen, J. Deng, Modified T-splines, *Computer Aided Geometric Design* 30 (9) (2013) 827–843.
- [22] J. Deng, F. Chen, X. Li, C. Hu, W. Tong, Z. Yang, Y. Feng, Polynomial splines over hierarchical T-meshes, *Graphical Models* 70 (2008) 76–86.
- [23] P. Wang, J. Xu, J. Deng, F. Chen, Adaptive isogeometric analysis using rational phT-splines, *Computer-Aided Design* 43 (11) (2011) 1438–1448.
- [24] A. Buffa, C. Giannelli, P. Morgenstern, D. Peterseim, Complexity of hierarchical refinement for a class of admissible mesh configurations, *Computer Aided Geometric Design* (2016) –doi:10.1016/j.cagd.2016.04.003.
- [25] C. Carstensen, M. Feischl, M. Page, D. Praetorius, Axioms of adaptivity, *Computers & Mathematics with Applications* 67 (6) (2014) 1195 – 1253. doi:10.1016/j.camwa.2013.12.003.
- [26] M. J. Borden, M. A. Scott, J. A. Evans, T. J. R. Hughes, Isogeometric finite element data structures based on Bézier extraction of NURBS, *Int. J. Numer. Meth. Engrg.* 87 (1-5) (2011) 15–47.
- [27] P. Hennig, S. Müller, M. Kästner, Bézier extraction and adaptive refinement of truncated hierarchical NURBS, *Computer Methods in Applied Mechanics and Engineering* (2016) –doi:10.1016/j.cma.2016.03.009.
- [28] L. Beirão da Veiga, A. Buffa, G. Sangalli, R. Vázquez, Analysis-suitable T-splines of arbitrary degree: definition, linear independence and approximation properties, *Mathematical Models and Methods in Applied Sciences* 23 (11) (2013) 1979–2003.
- [29] R. Verfürth, A review of a posteriori error estimation techniques for elasticity problems, *Computer Methods in Applied Mechanics and Engineering* 176 (1999) 419–440.
- [30] P. Binev, W. Dahmen, R. DeVore, Adaptive finite element methods with convergence rates, *Numerische Mathematik* 97 (2) (2004) 219–268. doi:10.1007/s00211-003-0492-7.

- [31] R. Stevenson, Optimality of a standard adaptive finite element method, *Foundations of Computational Mathematics* 7 (2) (2007) 245–269.
- [32] J. M. Cascon, C. Kreuzer, R. H. Nochetto, K. G. Siebert, Quasi-optimal convergence rate for an adaptive finite element method, *SIAM Journal on Numerical Analysis* 46 (5) (2008) 2524–2550.
- [33] L. Diening, C. Kreuzer, R. Stevenson, Instance optimality of the adaptive maximum strategy, *Foundations of Computational Mathematics* 16 (1) (2015) 33–68. doi:10.1007/s10208-014-9236-6.
- [34] C. Kreuzer, M. Schedensack, Instance optimal Crouzeix–Raviart adaptive finite element methods for the Poisson and Stokes problems, *IMA Journal of Numerical Analysis* (2015) drv019.
- [35] K. P. Gahalaut, S. K. Tomar, C. C. Douglas, Condition number estimates for matrices arising in NURBS based isogeometric discretizations of elliptic partial differential equations, arXiv:1406.6808.
- [36] Z. Yosibash, *Singularities in Elliptic Boundary Value Problems and Elasticity and Their Connection with Failure Initiation*, Springer New York, 2011.
- [37] H. Yserentant, On the multi-level splitting of finite element spaces, *Numerische Mathematik* 49 (4) (1986) 379–412.
- [38] S. Timoshenko, *Theory of Elasticity (McGraw-Hill Classic Textbook Reissue Series)*, 3rd Edition, McGraw-Hill Publishing Company, 1970.